A Soluble Metabolon Synthesizes the Isoprenoid Lipid Ubiquinone

Mahmoud Hajj Chehade, Ludovic Pelosi, Cameron David Fyfe, Laurent Loiseau, Bérengère Rascalou, Sabine Brugière, Katayoun Kazemzadeh, Chau-Duy-Tam Vo, Lidia Ciccone, Laurent Aussel, et al.

A soluble metabolon synthesizes the isoprenoid lipid Ubiquinone

Mahmoud Hajj Chehade[1], Ludovic Pelosi[1], Cameron David Fyfe[2], Laurent Loiseau[3], Bérengère Rascalou[1], Sabine Brugière[4], Katayoun Kazemzadeh[1], Chau-Duy-Tam Vo[2], Lidia Ciccone[5], Laurent Aussel[3], Yohann Couté[4], Marc Fontecave [2], Frédéric Barras[3, 6], Murielle Lombard[2], Fabien Pierrel [1]*

[1] Univ. Grenoble Alpes, CNRS, Grenoble INP, TIMC-IMAG, F-38000 Grenoble, France

[2] Laboratoire de Chimie des Processus Biologiques, Collège de France, Université Pierre et Marie Curie, CNRS UMR 8229, PSL Research University, 11 place Marcelin Berthelot, 75005 Paris, France.

[3] Aix Marseille Université, CNRS, Laboratoire Chimie Bactérienne, Institut Microbiologie de la Méditerranée, 31 Chemin Joseph Aiguier, Marseille 13009, France

[4] Univ. Grenoble Alpes, CEA, Inserm, BIG-BGE, 38000 Grenoble, France

[5] SOLEIL Synchrotron, L'Orme des Merisiers, 91198 Gif-sur-Yvette, France

[6] SAMe Unit, Department de Microbiologie, Institut Pasteur, 25 Rue du Dr Roux, 75015 Paris, France

* Correspondence: fabien.pierrel@univ-grenoble-alpes.fr

Lead contact: Fabien Pierrel

Key words: metabolon, multiprotein complex, lipid biosynthesis, ubiquinone, SCP2, metabolic pathway

ABSTRACT:

Ubiquinone (UQ) is a polyprenylated lipid that is conserved from bacteria to humans and is crucial to cellular respiration. How the cell orchestrates the efficient synthesis of UQ, which involves the modification of extremely hydrophobic substrates by multiple sequential enzymes, remains an unresolved issue. Here, we demonstrate that seven Ubi proteins form the Ubi complex, a stable metabolon that catalyzes the last six reactions of the UQ biosynthetic pathway in *Escherichia coli*. The SCP2 domain of UbiJ forms an extended hydrophobic cavity that binds UQ intermediates inside the 1 MDa Ubi complex. We purify the Ubi complex from cytoplasmic extracts and demonstrate that UQ biosynthesis occurs in this fraction, challenging the current thinking of a membrane-associated biosynthetic process. Collectively, our results document a rare case of stable metabolon and highlight how the supramolecular organization of soluble enzymes allows the modification of hydrophobic substrates in a hydrophilic environment.

INTRODUCTION:

Isoprenoid quinones are widespread in the three domains of life and represent a peculiar group of lipids able to undergo a two-step reversible redox process (Nowicka and Kruk, 2010). The electron transfer properties of isoprenoid quinones are essential to the function of respiratory chains that generate cellular ATP (Schoepp-Cothenet et al., 2013). Isoprenoid quinones also mediate disulfide bond formation in proteins (Bader et al., 2000), participate to virulence and antibiotic resistance in bacteria (Aussel et al., 2014b) and function as membrane soluble antioxidants (Bentinger et al., 2010; Nowicka and Kruk, 2010). The main isoprenoid quinones are menaquinone (MK) and ubiquinone (UQ), which is also called coenzyme Q in eukaryotes. MK and UQ share the same polyisoprenoid tail but differ by the structure of the redox-active head group, naphthalene ring and benzene ring, respectively (Figure S1A). The polyisoprenoid tail varies in length between organisms (UQ_6 in *Saccharomyces cerevisiae*, UQ_8 in *Escherichia coli* and UQ_{10} in humans) and confers extremely hydrophobic properties to isoprenoid quinones, which localize consequently in cellular membranes (Kawamukai, 2018; Nowicka and Kruk, 2010).

In the UQ biosynthesis pathway, the polyisoprenoid tail is added at an early step by an integral membrane polyprenyltransferase called UbiA in *E. coli* (Figure 1A). Subsequently, seven consecutive chemical reactions modify the head group to yield UQ (Figure 1A). Hydrophobic polyprenylated intermediates of the UQ biosynthetic pathway are predicted to be embedded within the lipid bilayer (Stefely and Pagliarini, 2017), with the head groups near the glycerol backbone of the membrane phospholipids and the isoprenoid tail inserted between their acyl chains (Galassi and Arantes, 2015; Hoyo et al., 2017; Wollstein et al., 2015). In contrast, the decarboxylase, methyltransferases and hydroxylases of the UQ biosynthetic pathway contain no transmembrane domains and are predicted to be soluble. Thus, how UQ biosynthetic enzymes overcome the biophysical barrier that separates them from their lipophilic substrates constitutes an unresolved issue.

Besides the Ubi enzymes that catalyze the chemical reactions of the pathway (Figure 1A), three Ubi proteins of unknown function are also required for efficient UQ biosynthesis, UbiB (Poon et al., 2000), UbiJ (Aussel et al., 2014a) and UbiK (Loiseau et al., 2017). Lately, we demonstrated that purified UbiJ and UbiK form a 1:2 heterocomplex that binds palmitoleic acid, one of *E. coli* most abundant fatty acid (Loiseau et al., 2017). This capacity to bind lipids suggested that UbiJ and UbiK may act as accessory factors of Ubi enzymes, but the role of these two proteins and of UbiB, although central for UQ biosynthesis, is still undefined (Bayly and Yadav, 2017; Loiseau et al., 2017; Reidenbach et al., 2017).

Together, UQ biosynthesis raises generic questions about how enzymes deal with extremely hydrophobic substrates and how cells orchestrate multi-step biosynthetic pathways. In order to address these fundamental questions, we have studied the subcellular localization and the structural organization of the UQ pathway in the bacterium *E. coli*. Here, we show that five Ubi enzymes and the accessory factors UbiJ-UbiK form a ~1000 kDa Ubi complex that resides in the cytosolic fraction. We demonstrate that UbiJ binds hydrophobic UQ biosynthetic intermediates and is also the keystone of the Ubi complex. Our work describes the Ubi complex as a unique microreactor, which enables the multistep biosynthesis of a complex lipid in a hydrophilic cellular environment.

RESULTS:

UQ biosynthesis takes place in the soluble fraction of E. coli lysates

An assay to monitor UQ biosynthesis *in vitro* is not available (Stefely and Pagliarini, 2017). We designed an *in vivo* experimental approach to accumulate a labelled version of OPP within cells and to monitor its conversion into labelled UQ. We transferred Δ*ubiC* cells pretreated with chloramphenicol in an O_2-free atmosphere and added the labelled precursor $^{13}C_7$-4HB. The absence of dioxygen blocked UQ biosynthesis (Shestopalov et al., 1997), and the cells quickly accumulated $^{13}C_6$-OPP (Figure S1B). Upon exposure to air, cells preloaded anaerobically with $^{13}C_6$-OPP synthesized $^{13}C_6$-UQ_8 (Figure S1C).

Conversely, we observed no $^{13}C_6$-UQ_8 synthesis in cells maintained under argon atmosphere (Figure S1C). Thus, dioxygen triggered the *in vivo* conversion of $^{13}C_6$-OPP into $^{13}C_6$-UQ_8 in our experimental set-up, in agreement with the hydroxylases UbiF, H and UbiI requiring O_2 as a cosubstrate (Alexander and Young, 1978; Hajj Chehade et al., 2013) (Figure 1A).

Next, we lysed cells loaded with $^{13}C_6$-OPP and found that total cell free extracts incubated under air at 30°C also synthesized $^{13}C_6$-UQ_8 (Figure S1D). The biosynthesis of UQ_8 was strongly stimulated by the addition of S-adenosylmethionine and NADH (Figure S1D), which act respectively as the methyl-donor for the methylation reactions and as the electron-donor for the hydroxylases (Knoell, 1979b). Finally, we fractionated the cell free extracts by ultracentrifugation and assayed the cytoplasmic and membrane fractions for UQ biosynthesis. Only the cytoplasmic fraction produced $^{13}C_6$-UQ_8 upon exposure to air (Figure 1B and S1E). The initial rates were comparable between the soluble fraction and cell free extracts (Figure 1B). However increased $^{13}C_6$-UQ_8 synthesis was observed at later stages in cell free extracts (Figure 1B), potentially reflecting limiting amounts of the $^{13}C_6$-OPP substrate in the soluble fraction. In conclusion, we developed an activity assay, which strongly supports that the last six reactions of the UQ biosynthetic pathway take place in the cytosol.

Ubi proteins are found predominantly in the soluble fraction of E. coli lysates

The presence of UQ biosynthesis activity in the cytoplasmic fraction prompted us to evaluate the distribution of Ubi proteins. We created several Ubi-SPA strains by inserting a sequence coding for the SPA tag at the 3' end of *ubi* genes in the *E. coli* chromosome (Figure S1F). The tagged proteins were functional since the UQ_8 content of the strains accounted for at least 70% of WT level (Figure S1G). Western blot analysis of cellular extracts with an anti-Flag antibody detected the Ubi proteins at their expected size, except the membrane-bound UbiA and UbiB that did not show any signal (data not shown). Ultracentrifugation of cell free extracts separated soluble and membrane fractions as verified by immunodetection of the cytosolic glyceraldehyde 3-phosphate dehydrogenase (GAPDH) and the membrane-bound porin LamB (Figure 1C). All tested Ubi-SPA proteins distributed in both fractions

(Figure 1C). We calculated the total amount of each Ubi protein in the entire soluble and membrane fractions. The ratio of these amounts indicate the distribution of each Ubi protein (Figure 1C) and showed that all Ubi proteins localized predominantly in the soluble fraction, except UbiK.

Seven Ubi proteins form a 1 MDa complex

To further characterize the soluble Ubi proteins, we analyzed cytoplasmic fractions by Blue Native PAGE (BN-PAGE), a technique that preserves the integrity of protein complexes and separates them according to their hydrodynamic size and shape (Wittig et al., 2006). Anti-Flag immunodetection showed that seven Ubi-SPA proteins (UbiE, F, G, H, I, J, K) co-migrated at ~1000 kDa, whereas UbiD and UbiX co-migrated at around 700 kDa (Figure 2A). Similar results were obtained with an anti-CBP antibody, demonstrating the specific detection of the SPA tag fused to the Ubi proteins (Figure S2A). As expected, the tetrameric GAPDH protein (4x35.5 kDa) ran at ~140 kDa (Figure 2A and S2A). We also subjected the samples to a denaturating second dimension electrophoresis (2D SDS-PAGE) after the first dimension BN-PAGE (1D BN-PAGE). 2D SDS-PAGE confirmed the migration of UbiE, F, G, H, I, J, K proteins at ~1000 kDa and of UbiX and UbiD at ~700 kDa (Figure 2B). GAPDH was detected at ~100 kDa with variations between experiments due to migration artefacts in the lower part of the gel and to disparities in the positioning of the 1D BN-PAGE lane (Figure S2B).

To corroborate the co-migration of several Ubi proteins, we used a second method that separates proteins in glycerol gradients according to their density. UbiE, F, G, H, I, J, K distributed around the high density fractions 11 to 16, whereas UbiD and X were most abundant in fractions 9 to 13, and GAPDH eluted in fractions 6 to 10 (Figure 2C). Silver staining revealed that most proteins of the soluble extracts localized in low-density fractions (Figure 2C). We analyzed by 2D SDS-PAGE fractions 11, 12 and 13 from the glycerol gradient of UbiG-SPA and obtained a signal for the UbiG protein at ~1000 kDa (Figure 2D). Thus, both BN-PAGE and glycerol gradient experiments consistently established the existence of the same protein complex that we name “Ubi complex”.

To provide additional proof of the existence of the Ubi complex, we performed bacterial two-hydrid experiments, in which adenylate cyclase (AC) activity reports on the interaction between Ubi proteins fused either to the T18 or T25 domains of AC (Karimova et al., 1998). We tested all combinations (Table S1) and obtained an interaction network where the seven proteins of the Ubi complex exhibited multiple robust interactions, whereas the other Ubi proteins were less connected (Figure 2E). Collectively, our results are consistent with UbiE, F, G, H, I, J, K being part of a cytoplasmic 1 MDa Ubi complex, whereas UbiX and UbiD involved in the decarboxylation step form a separate entity.

Purification of the Ubi complex and identification of its components

Next, we isolated the Ubi complex using sequential affinity purification, a two-step procedure that uses first the FLAG epitopes of the SPA tag and second its CBP domain (Babu et al., 2009). We processed soluble extracts from UbiE-SPA cells and from WT untagged cells as control. Both eluates from the anti-FLAG resin were similar (Figure S2C-D) but immunodetection confirmed the presence of UbiE-CBP in the UbiE-SPA sample (Figure S2E). E2-E4 eluates of the calmodulin resin showed multiple bands that were absent in the control eluate (Figure S2F-G) and contained the bait UbiE-CBP protein as revealed by western blot analysis (Figure S2H). We detected the purified Ubi complex at ~1000 kDa in a 2D SDS-PAGE analysis of the E2 eluate (Figure 3A), with a signal similar to the Ubi complex in total soluble fractions (Figure 2B). We similarly purified the Ubi complex from UbiI-SPA and UbiG-SPA strains and obtained E2 fractions whose SDS-PAGE shared protein bands with the UbiE-SPA fraction E2 (Figure 3B). To identify the proteins in the Ubi complex, all three samples were submitted to mass spectrometry (MS)-based proteomic analysis and compared with E2 fractions from independent control purifications. The stringent comparison of MS-based results obtained for SPA-tagged proteins and negative controls identified several proteins that co-purified with the bait proteins (Table S2). Interestingly we detected only seven Ubi proteins and all of them were found in a subset of 8 proteins systematically enriched in the three Ubi-SPA eluates (Figure 3C, Table S2). The 8 proteins were UbiE,

F, G, H, I, J, K and the lipoprotein Blc, which physiological function remains uncertain (Campanacci et al., 2006). The UQ_8 content of the Δ*blc* strain was comparable to WT (Figure S2I), showing that the Blc protein is not required for UQ biosynthesis, unlike Ubi proteins of the Ubi complex. Overall, we conclude that the biosynthesis of UQ in the soluble fraction (Figure 1B) is mediated by the Ubi complex, which contains the five enzymes (UbiE, F, G, H, I) necessary to convert OPP to UQ_8 (Figure 1A) and two accessory factors, UbiJ and UbiK.

UQ biosynthetic intermediates OPP and DMQ_8 co-elute with the Ubi complex

Using HPLC coupled to electrochemical detection and mass spectrometry (HPLC-ECD-MS), we analyzed the distribution of isoprenoid quinones in exponentially growing *E. coli* cells and found that the UQ intermediates OPP and DMQ_8 accumulated substantially in the cytosolic fraction, whereas UQ_8 was highly enriched in the membrane fraction (Figure 4A). Analysis of the cytosols of Ubi-SPA strains on glycerol gradients revealed that OPP and DMQ_8 were enriched in fractions that contain the Ubi complex, as visualized by western-blot analysis (Figure 4B and S3A-B). Conversely, UQ_8 distributed quite evenly in the gradient (Figure 4B and S3A-B). Together, these results showed that the hydrophobic intermediates OPP and DMQ_8 localized to a significant extent in the soluble fraction of *E. coli* extracts and co-eluted with the Ubi complex.

The SCP2 domain of UbiJ binds isoprenoid lipids

We recently showed that the purified UbiJ-UbiK heterocomplex binds palmitoleic acid (Loiseau et al., 2017), one of the most abundant fatty acid in *E. coli*. Overexpression of UbiJ-K caused a decrease in cellular UQ_8 levels and the accumulation of OPP and DMQ_8 (Figure 4C and S3C), suggesting the sequestration of these UQ_8 biosynthetic intermediates by UbiJ-K. We then purified the UbiJ-K complex (Figure S3D) using affinity chromatography and size-exclusion chromatography, and analyzed its quinone content by HPLC-ECD-MS (Figure S3E). We detected UQ_8, OPP and DMQ_8 (Figure 4D), showing that UbiJ-K is able to bind all three isoprenoid lipids. To elucidate which of the two proteins is responsible for lipid binding, we purified UbiK and the N-terminal SCP2 domain of UbiJ (UbiJ-SCP2)

(Figure S5E); full-length UbiJ was not amenable to purification. We detected UQ_8, OPP and DMQ_8 in UbiJ-SCP2, but not in UbiK samples (Figure 4D and S3E). The calculated UQ_8 /protein ratio showed a low occupancy in UbiJ-K and UbiJ-SCP2 (less than 0.3 %), probably due to the high yield expression and the multiple purification steps. Together, our results strongly support that the SCP2 domain of UbiJ, and not UbiK, is responsible for binding UQ_8 and the biosynthetic intermediates OPP and DMQ_8 in the Ubi complex.

Structure of the SCP2 domain of UbiJ

UbiJ-SCP2 behaved as a dimer in solution and crystallized in the space group P212121 with an asymmetric unit containing either a dimer or a tetramer (Table S3). The structure shown in Figure 5A is that of the dimer generated with data collected to the highest 1.7 Å resolution. An electron density map is shown in Figure S4. The protein has an α/β-fold with 5 α-helices and 5 β-strands forming a hydrophobic center with an open cavity (Figure 5B). The walls of this cavity are composed of hydrophobic residues provided both by the α-helices and the β-strands (Figure 5C-D). It is interesting to note that, at those specific positions, UbiJ-SCP2 domains have exclusively hydrophobic residues (Figure S5). The overall structure, as well as the presence of a hydrophobic cavity, is highly reminiscent of previously reported structures of the SCP2 protein family (Table S4). This suggests that the absence of the C-terminal part of UbiJ does not perturb the SCP2 domain in line with our model showing two independent domains (Loiseau et al., 2017). In some cases, SCP2 proteins have been crystallized in complex with a hydrophobic ligand as a further evidence for the cavity playing a functional role in lipid binding (Table S4) (Burgardt et al., 2017; De Berti et al., 2013; Dyer et al., 2008; Haapalainen et al., 2001). Although the model we present does not contain any ligand, electron density was noted within the cavity (Figure 5C). It is tempting to suggest that this unexplained density is related to the various lipids detected in small quantities within the purified protein (see above) and that the cavity of UbiJ serves as the binding site for UQ_8 intermediates. As a final support to that hypothesis we found that a UQ_8 conformation taken from a previously reported structure of photosynthetic LH1-RC protein in

complex with UQ_8 (Yu et al., 2018) nicely aligns into this cavity, with a reasonable fit in length (Figure 5E).

UbiJ is essential to the stability of the Ubi complex

Our characterization of UbiJ as a polyprenyl lipid-binding protein led us to characterize OPP binding to the Ubi complex in Δ*ubiJ* cells. Δ*ubiJ* cells are blocked at an undefined early step of the UQ biosynthetic pathway (Aussel et al., 2014a) and have therefore a strongly diminished UQ_8 content and increased OPP levels compared to WT cells (Figure S6A). The cytosol of UbiG-SPA Δ*ubiJ* cells analyzed on glycerol gradient showed a profile with comparable amounts of OPP and UQ_8 in all fractions (Figure 6a). A similar result was obtained with UbiF-SPA Δ*ubiJ* and UbiH-SPA Δ*ubiJ* cells (Figure S6B-C). This distribution of OPP is in stark contrast with the accumulation of OPP in the Ubi complex observed in cells that contain UbiJ (Figure 4B and S3A-B).

The deletion of *ubiJ* did not affect the steady state level of UbiF or UbiG but lowered that of UbiH (Figure S6B). Western-blot analyses revealed that the Ubi proteins shifted from fractions 11-16 (Figure 2c) in WT cells to fractions 2-10 in Δ*ubiJ* cells (Figure 6A and S6C-D), whereas the position of GAPDH was unchanged (compare Figure 6A and 2C). BN-PAGE and 2D-SDS-PAGE analyses showed that the Ubi complex was absent in Δ*ubiJ* cells (Figure 6B-D). Conversely, the Ubi complex was readily detected in cells lacking *ubiE*, *ubiF*, *ubiG* (Figure 6B-C) or *ubiK* (Figure 6E), even though deletion of this last gene decreased UbiI levels (Figure S6E). Interestingly, cells with a Ubi complex lacking an enzymatic subunit like UbiF or UbiE produced substantial quantities of the late stage intermediates DMQ_8 and $DDMQ_8$, respectively (Figure S6F). Together, our results show that UbiJ is required for the stability of the Ubi complex and explain why UQ biosynthesis cannot progress past the early intermediate OPP in Δ*ubiJ* cells.

DISCUSSION:

Here, we demonstrate the supramolecular organization of seven UQ biosynthesis proteins in a 1 MDa Ubi complex (Figure 2), which is remarkable for at least 2 reasons. First, it constitutes a stable metabolon, a term that designates the association of sequential enzymes acting in a metabolic pathway (Srere, 1985). Often, metabolons are highly dynamic and therefore not amenable to biochemical characterization (Laursen et al., 2016; Nguyen et al., 2014; Wu and Minteer, 2015), like the purinosome. However, a few stable metabolons have been purified like the pyruvate dehydrogenase complex (Zhou et al., 2001) or a triacylglycerol biosynthetic complex in *Rhodotorula glutinis* (Gangar et al., 2001). We have shown that the Ubi complex contains two accessory factors (UbiJ, K) and the Ubi enzymes (UbiI, G, H, E, F) that catalyze the last six reactions of the UQ biosynthesis pathway. As such, the Ubi complex is, to our knowledge, ~~the first example of a~~the stable metabolon that ~~coordinating~~ coordinates the ~~so many~~highest number of chemical reactions. Substrate channeling between Ubi enzymes and control of undesired reactivity of UQ intermediates may be conferred by the Ubi metabolon to contribute to efficient UQ biosynthesis.

Second, the Ubi complex is present in the cytosolic fraction even though its polyprenylated substrates count among the most hydrophobic molecules in life (Nowicka and Kruk, 2010; Stefely and Pagliarini, 2017). As a matter of fact, we have experimentally established that the biosynthetic steps from OPP to UQ_8 proceed in the cytosolic fraction, independently from the membrane, as suggested by an early report (Knoell, 1979a) and supported by the following results: i) OPP and DMQ_8, two UQ_8 biosynthetic intermediates, accumulated in the cytosolic fraction to a greater extent than the mature UQ_8 and co-purified with the soluble Ubi complex (Figure 4), ii) the Ubi metabolon was located in the soluble fraction, which actively converted OPP into UQ_8 *in vitro*, unlike the membrane fraction (Figure 1B). We believe that UbiJ is key to create, in the Ubi complex, a microenvironment that isolates lipophilic molecules from the surrounding hydrophilic cytoplasm. Indeed, we demonstrated that the SCP2 domain of UbiJ binds UQ biosynthetic intermediates (Figure 4) and the crystal structure revealed

an elongated hydrophobic cavity, which size and shape is compatible with the binding of the polyprenyl tail of UQ intermediates (Figure 5). SCP2 domains are typically found lone (unfused) or in multidomain proteins and fulfill lipid-binding and transport functions in all domains of life (Burgardt et al., 2017). We demonstrated here ~~for the first time~~ the presence of a SCP2 protein in a multiprotein complex involved in lipid modification. Altogether, we propose a model of UQ_8 biosynthesis, in which the hydrophobic UQ intermediates downstream of OPP are not associated to membrane lipids but to UbiJ within the soluble Ubi metabolon (Figure 6F).

Since the early prenylation step by UbiA takes place in the membrane (Cheng and Li, 2014; Huang et al., 2014), our model postulates that the early octaprenyl intermediates (either OHB or OPP) move out of the membrane so that OPP can bind to UbiJ in the soluble Ubi complex. This mechanism is unusual because enzymes that synthesize lipids are often membrane-bound or membrane-associated, like the phospholipid biosynthetic pathways in *E. coli* (Lopez-Lara and Geiger, 2017). However, the extrusion of a lipid from the membrane to allow its chemical modification has a precedent, with the eukaryotic Sec14 that extracts phosphatidylinositol from the membrane and presents it to soluble hydroxylases (Bankaitis et al., 2010). In the case of UQ biosynthesis, we believe that the accessory factor UbiB may assist the extrusion of either OHB or OPP from the membrane (Figure 6F). Indeed, UbiB and its eukaryote homolog Coq8 were recently hypothesized to couple the hydrolysis of ATP to the extraction of head groups of UQ intermediates out of the membrane (Reidenbach et al., 2017; Stefely et al., 2016). Of note, UbiB contains one transmembrane domain and is not part of the purified Ubi complex (Table S2), consistent with the soluble nature of the latter. Reciprocally, how UQ_8 is delivered to the membrane bilayer after its synthesis by the soluble Ubi complex will be addressed in future studies. Overall, UbiK may also play a role in trafficking the polyprenyl molecules in and out of the membrane as a significant part of UbiK associates with the membrane (Figure 1C) and it was described to enhance the fusion of membranes *in vitro* (Carrica et al., 2011).

279 UbiJ and UbiK are conserved in many proteobacteria (Loiseau et al., 2017; Xia et al., 2017) and
280 we demonstrated that both proteins are *bona fide* subunits of the Ubi complex. Besides binding UQ
281 intermediates, we also found that UbiJ was an essential structural element of the Ubi complex, unlike
282 other Ubi proteins (Figure 6B-E). We showed previously that the C-terminal domain of UbiJ was
283 essential for UQ biosynthesis *in vivo* and formed an extended α-helix that likely associated within a
284 three-helix bundle in the $UbiK_2$-$UbiJ_1$ heterocomplex (Aussel et al., 2014a; Loiseau et al., 2017). Taking
285 all these findings into account, we propose that UbiJ is the keystone of the Ubi complex and constitutes
286 a docking platform where Ubi enzymes assemble and access their SCP2-bound polyprenyl substrates.
287 The total molecular weight of the eight proteins identified in the purified Ubi complex approaches 270
288 kDa, still far from the estimated 1 MDa observed on BN-PAGE. The extra mass may correspond to
289 multimeres of Ubi proteins in the Ubi complex, as supported by a study that found members of
290 multiprotein complexes to be made in precise proportion to their stoichiometry, and showed that Ubi
291 proteins have heterogeneous synthesis rates (Li et al., 2014). We also found that several Ubi proteins
292 interacted with themselves in our two-hybrid assay (Table S1), supporting that they may multimerize.

293 Based on the conservation of Ubi proteins, it is tempting to suggest that the UQ biosynthetic
294 pathway of many proteobacteria is organized around a soluble stable metabolon, like in *E. coli*.
295 Nonetheless, we expect different versions of the Ubi complex across proteobacteria because of
296 variations in the number of UQ hydroxylases (Pelosi et al., 2016) and of other components of the
297 pathway (Esposti, 2017). In eukaryotes, it is unclear whether a UQ biosynthesis metabolon exists since
298 enzymes are still missing for two chemical reactions of the pathway (Awad et al., 2018). BN-PAGE
299 experiments showed that several UQ biosynthetic proteins form a complex associated with the
300 mitochondrial inner membrane in the yeast *S. cerevisiae* (He et al., 2014; Marbois et al., 2009), and
301 such supramolecular organization may also exist in mammalian cells (Floyd et al., 2016; Stefely et al.,
302 2016). However, the composition of the complex is uncertain since multiple proteins not related to UQ
303 biosynthesis co-purified with yeast UQ biosynthetic proteins (Allan et al., 2015). Interestingly, two UQ
304 biosynthesis proteins of unknown function and restricted to eukaryotes, Coq4 and Coq9, are able to

bind lipids (Lohman et al., 2014; Rea et al., 2010) and exhibit genetic interactions with other Coq proteins (Hsieh et al., 2007; Marbois et al., 2009; Ozeir et al., 2015). We suspect that Coq4 and Coq9 may chaperone UQ intermediates, similar to bacterial UbiJ.

In conclusion, we discovered a stable metabolon - the Ubi complex - that catalyzes UQ biosynthesis, thanks to the association of five enzymes and two accessory factors. Surprisingly this metabolon localizes in the cytosolic fraction of *E. coli*, despite the extreme hydrophobicity of UQ biosynthetic intermediates. Our work shows that the SCP2 protein UbiJ binds these compounds and opens new questions regarding the trafficking of polyprenyl lipids in and out of membranes. The Ubi complex microreactor represents also a fascinating model to study how substrates are sequentially processed by multiple active sites located in a single structural entity.

SIGNIFICANCE

Ubiquinone is a conserved isoprenoid lipid of crucial physiological importance. Isoprenoid intermediates in ubiquinone biosynthesis are extremely hydrophobic; thus the pathway is proposed to be membrane-associated. Unexpectedly, we demonstrate that most steps in bacterial UQ biosynthesis are independent of the membrane and occur inside a soluble multiprotein complex that forms a stable metabolon. We elucidate a key role for the SCP2 domain of the UbiJ protein in binding the isoprenoid intermediates inside the multiprotein complex, documenting that~~the first example of~~ the widespread SCP2 domain also functions in assisting chemical modifications of lipids. Our work highlights a remarkable bacterial metabolon synthesizing the hydrophobic ubiquinone molecule in the cytosol, and raises questions regarding the trafficking of isoprenoid lipids in and out of the membrane.

ACKNOWLEDGEMENTS

This work was supported by the Agence Nationale de la Recherche (ANR), ANR Blanc (An)aeroUbi ANR-15-CE11-0001-02. We thank Amélie Amblard and Mikael Martin for technical assistance and the GEM team at TIMC for discussions and suggestions. SB and YC thank the support of the discovery platform and data science group at EDyP. Proteomic experiments were partly supported by the Proteomics French Infrastructure (ANR-10-INBS-08-01 grant) and the Labex GRAL (ANR-10-LABX-49-01). Diffraction data were collected at the synchrotron SOLEIL, beamlines Proxima 1 and Proxima 2 (Saint-Aubin, France). We are most grateful to the beamline scientists, in particular Pierre Legrand and Bill Sheperd. CF, CDTV, ML and MF acknowledge support from the French National Research Agency (Labex program DYNAMO, ANR-11-LABX-0011) and from Fondation de l'Orangerie for Individual Philanthropy.

AUTHOR CONTRIBUTIONS

FP, LP, MF, FB, ML, MHC designed research and FP coordinated the project. All authors performed experiments and/or data analysis. FP, LP, MF, FB, ML, and MHC wrote the paper and the manuscript was reviewed by all authors.

DECLARATION OF INTERESTS

The authors declare no competing interests.

REFERENCES

Alberge, F., Espinosa, L., Seduk, F., Sylvi, L., Toci, R., Walburger, A., and Magalon, A. (2015). Dynamic subcellular localization of a respiratory complex controls bacterial respiration. Elife *4*.

Alexander, K., and Young, I.G. (1978). Three hydroxylations incorporating molecular oxygen in the aerobic biosynthesis of ubiquinone in Escherichia coli. Biochemistry *17*, 4745-4750.

Allan, C.M., Awad, A.M., Johnson, J.S., Shirasaki, D.I., Wang, C., Blaby-Haas, C.E., Merchant, S.S., Loo, J.A., and Clarke, C.F. (2015). Identification of Coq11, a new coenzyme Q biosynthetic protein in the CoQ-synthome in Saccharomyces cerevisiae. J. Biol. Chem. *290*, 7517-7534.

Aussel, L., Loiseau, L., Hajj Chehade, M., Pocachard, B., Fontecave, M., Pierrel, F., and Barras, F. (2014a). ubiJ, a New Gene Required for Aerobic Growth and Proliferation in Macrophage, Is

Involved in Coenzyme Q Biosynthesis in Escherichia coli and Salmonella enterica Serovar Typhimurium. J. Bacteriol. *196*, 70-79.
Aussel, L., Pierrel, F., Loiseau, L., Lombard, M., Fontecave, M., and Barras, F. (2014b). Biosynthesis and physiology of coenzyme Q in bacteria. Biochim. Biophys. Acta *1837*, 1004-1011.
Awad, A.M., Bradley, M.C., Fernandez-Del-Rio, L., Nag, A., Tsui, H.S., and Clarke, C.F. (2018). Coenzyme Q10 deficiencies: pathways in yeast and humans. Essays Biochem.
Baba, T., Ara, T., Hasegawa, M., Takai, Y., Okumura, Y., Baba, M., Datsenko, K.A., Tomita, M., Wanner, B.L., and Mori, H. (2006). Construction of Escherichia coli K-12 in-frame, single-gene knockout mutants: the Keio collection. Mol. Syst. Biol. *2*, 2006 0008.
Babu, M., Butland, G., Pogoutse, O., Li, J., Greenblatt, J.F., and Emili, A. (2009). Sequential peptide affinity purification system for the systematic isolation and identification of protein complexes from Escherichia coli. Methods Mol Biol *564*, 373-400.
Bader, M.W., Xie, T., Yu, C.A., and Bardwell, J.C. (2000). Disulfide bonds are generated by quinone reduction. J. Biol. Chem. *275*, 26082-26088.
Bankaitis, V.A., Mousley, C.J., and Schaaf, G. (2010). The Sec14 superfamily and mechanisms for crosstalk between lipid metabolism and lipid signaling. Trends Biochem. Sci. *35*, 150-160.
Barral, S., Morozumi, Y., Tanaka, H., Montellier, E., Govin, J., de Dieuleveult, M., Charbonnier, G., Coute, Y., Puthier, D., Buchou, T.*, et al.* (2017). Histone Variant H2A.L.2 Guides Transition Protein-Dependent Protamine Assembly in Male Germ Cells. Mol. Cell *66*, 89-101 e108.
Bayly, C.L., and Yadav, V.G. (2017). Towards Precision Engineering of Canonical Polyketide Synthase Domains: Recent Advances and Future Prospects. Molecules *22*, 18.
Bentinger, M., Tekle, M., and Dallner, G. (2010). Coenzyme Q-biosynthesis and functions. Biochem. Biophys. Res. Commun. *396*, 74-79.
Bricogne, G., Blanc, E., Brandl, M., Flensburg, C., Keller, P., Paciorek, W., Roversi, P., Sharff, A., Smart, O.S., Vonrhein, C.*, et al.* (2017). BUSTER version 2.10.2. Cambridge, United Kingdom: Global Phasing Ltd.
Burgardt, N.I., Gianotti, A.R., Ferreyra, R.G., and Ermacora, M.R. (2017). A structural appraisal of sterol carrier protein 2. Biochimica Et Biophysica Acta-Proteins and Proteomics *1865*, 565-577.
Campanacci, V., Bishop, R.E., Blangy, S., Tegoni, M., and Cambillau, C. (2006). The membrane bound bacterial lipocalin Blc is a functional dimer with binding preference for lysophospholipids. FEBS Lett. *580*, 4877-4883.
Carrica, M.C., Craig, P.O., Garcia-Angulo, V.A., Aguirre, A., Garcia-Vescovi, E., Goldbaum, F.A., and Cravero, S.L. (2011). YqiC of Salmonella enterica serovar Typhimurium is a membrane fusogenic protein required for mice colonization. BMC Microbiol *11*, 95.
Cheng, W., and Li, W. (2014). Structural insights into ubiquinone biosynthesis in membranes. Science *343*, 878-881.
Chovancova, E., Pavelka, A., Benes, P., Strnad, O., Brezovsky, J., Kozlikova, B., Gora, A., Sustr, V., Klvana, M., Medek, P.*, et al.* (2012). CAVER 3.0: a tool for the analysis of transport pathways in dynamic protein structures. PLoS Comput. Biol. *8*, e1002708.
Cowtan, K. (2006). The Buccaneer software for automated model building. 1. Tracing protein chains. Acta Crystallogr D Biol Crystallogr *62*, 1002-1011.
De Berti, F.P., Capaldi, S., Ferreyra, R., Burgardt, N., Acierno, J.P., Klinke, S., Monaco, H.L., and Ermacora, M.R. (2013). The crystal structure of sterol carrier protein 2 from Yarrowia lipolytica and the evolutionary conservation of a large, non-specific lipid-binding cavity. J. Struct. Funct. Genomics *14*, 145-153.
Dyer, D.H., Wessely, V., Forest, K.T., and Lan, Q. (2008). Three-dimensional structure/function analysis of SCP-2-like2 reveals differences among SCP-2 family members. J. Lipid Res. *49*, 644-653.
Emsley, P., Lohkamp, B., Scott, W.G., and Cowtan, K. (2010). Features and development of Coot. Acta Crystallogr D Biol Crystallogr *66*, 486-501.

Esposti, M.D. (2017). A journey across genomes uncovers the origin of ubiquinone in cyanobacteria. Genome Biol Evol.
Floyd, B.J., Wilkerson, E.M., Veling, M.T., Minogue, C.E., Xia, C., Beebe, E.T., Wrobel, R.L., Cho, H., Kremer, L.S., Alston, C.L., *et al.* (2016). Mitochondrial Protein Interaction Mapping Identifies Regulators of Respiratory Chain Function. Mol. Cell *63*, 621-632.
Galassi, V.V., and Arantes, G.M. (2015). Partition, orientation and mobility of ubiquinones in a lipid bilayer. Biochimica Et Biophysica Acta-Bioenergetics *1847*, 1560-1573.
Gangar, A., Karande, A.A., and Rajasekharan, R. (2001). Isolation and localization of a cytosolic 10 S triacylglycerol biosynthetic multienzyme complex from oleaginous yeast. J. Biol. Chem. *276*, 10290-10298.
Haapalainen, A.M., van Aalten, D.M., Merilainen, G., Jalonen, J.E., Pirila, P., Wierenga, R.K., Hiltunen, J.K., and Glumoff, T. (2001). Crystal structure of the liganded SCP-2-like domain of human peroxisomal multifunctional enzyme type 2 at 1.75 A resolution. J. Mol. Biol. *313*, 1127-1138.
Hajj Chehade, M., Loiseau, L., Lombard, M., Pecqueur, L., Ismail, A., Smadja, M., Golinelli-Pimpaneau, B., Mellot-Draznieks, C., Hamelin, O., Aussel, L., *et al.* (2013). ubiI, a New Gene in Escherichia coli Coenzyme Q Biosynthesis, Is Involved in Aerobic C5-hydroxylation. J. Biol. Chem. *288*, 20085-20092.
He, C.H., Xie, L.X., Allan, C.M., Tran, U.C., and Clarke, C.F. (2014). Coenzyme Q supplementation or over-expression of the yeast Coq8 putative kinase stabilizes multi-subunit Coq polypeptide complexes in yeast coq null mutants. Biochim. Biophys. Acta *1841*, 630-644.
Hoyo, J., Guaus, E., and Torrent-Burgues, J. (2017). Tuning ubiquinone position in biomimetic monolayer membranes. European Physical Journal E *40*.
Hsieh, E.J., Gin, P., Gulmezian, M., Tran, U.C., Saiki, R., Marbois, B.N., and Clarke, C.F. (2007). *Saccharomyces cerevisiae* Coq9 polypeptide is a subunit of the mitochondrial coenzyme Q biosynthetic complex. Arch. Biochem. Biophys. *463*, 19-26.
Hu, P.Z., Janga, S.C., Babu, M., Diaz-Mejia, J.J., Butland, G., Yang, W.H., Pogoutse, O., Guo, X.H., Phanse, S., Wong, P., *et al.* (2009). Global Functional Atlas of Escherichia coli Encompassing Previously Uncharacterized Proteins. PLoS Biol. *7*, 929-947.
Huang, H., Levin, E.J., Liu, S., Bai, Y., Lockless, S.W., and Zhou, M. (2014). Structure of a Membrane-Embedded Prenyltransferase Homologous to UBIAD1. PLoS Biol. *12*, e1001911.
Kabsch, W. (2010). Xds. Acta Crystallogr D Biol Crystallogr *66*, 125-132.
Karimova, G., Pidoux, J., Ullmann, A., and Ladant, D. (1998). A bacterial two-hybrid system based on a reconstituted signal transduction pathway. Proc. Natl. Acad. Sci. U. S. A. *95*, 5752-5756.
Kawamukai, M. (2018). Biosynthesis and applications of prenylquinones. Biosci. Biotechnol. Biochem. *82*, 963-977.
Knoell, H.E. (1979a). Isolation of a soluble enzyme complex comprising the ubiquinone-8 synthesis apparatus from the cytoplasmic membrane of Escherichia coli. Biochem. Biophys. Res. Commun. *91*, 919-925.
Knoell, H.E. (1979b). Ubiquinone synthesis in vitro starting from 2-octaprenyl phenol. FEBS Lett. *97*, 155-158.
Laursen, T., Borch, J., Knudsen, C., Bavishi, K., Torta, F., Martens, H.J., Silvestro, D., Hatzakis, N.S., Wenk, M.R., Dafforn, T.R., *et al.* (2016). Characterization of a dynamic metabolon producing the defense compound dhurrin in sorghum. Science *354*, 890-893.
Li, G.W., Burkhardt, D., Gross, C., and Weissman, J.S. (2014). Quantifying absolute protein synthesis rates reveals principles underlying allocation of cellular resources. Cell *157*, 624-635.
Lohman, D.C., Forouhar, F., Beebe, E.T., Stefely, M.S., Minogue, C.E., Ulbrich, A., Stefely, J.A., Sukumar, S., Luna-Sanchez, M., Jochem, A., *et al.* (2014). Mitochondrial COQ9 is a lipid-binding protein that associates with COQ7 to enable coenzyme Q biosynthesis. Proc. Natl. Acad. Sci. U. S. A. *111*, E4697-4705.
Loiseau, L., Fyfe, C., Aussel, L., Hajj Chehade, M., Hernandez, S.B., Faivre, B., Hamdane, D., Mellot-Draznieks, C., Rascalou, B., Pelosi, L., *et al.* (2017). The UbiK protein is an accessory factor

necessary for bacterial ubiquinone (UQ) biosynthesis and forms a complex with the UQ biogenesis factor UbiJ. J. Biol. Chem. *292*, 11937-11950.
Lopez-Lara, I.M., and Geiger, O. (2017). Bacterial lipid diversity. Biochimica Et Biophysica Acta-Molecular and Cell Biology of Lipids *1862*, 1287-1299.
Marbois, B., Gin, P., Gulmezian, M., and Clarke, C.F. (2009). The yeast Coq4 polypeptide organizes a mitochondrial protein complex essential for coenzyme Q biosynthesis. Biochim. Biophys. Acta *1791*, 69-75.
Nguyen, C., Haushalter, R.W., Lee, D.J., Markwick, P.R.L., Bruegger, J., Caldara-Festin, G., Finzel, K., Jackson, D.R., Ishikawa, F., O'Dowd, B.*, et al.* (2014). Trapping the dynamic acyl carrier protein in fatty acid biosynthesis. Nature *505*, 427-431.
Nowicka, B., and Kruk, J. (2010). Occurrence, biosynthesis and function of isoprenoid quinones. Biochim. Biophys. Acta *1797*, 1587-1605.
Ozeir, M., Pelosi, L., Ismail, A., Mellot-Draznieks, C., Fontecave, M., and Pierrel, F. (2015). Coq6 Is Responsible for the C4-deamination Reaction in Coenzyme Q Biosynthesis in Saccharomyces cerevisiae. J. Biol. Chem. *290*, 24140-24151.
Pavelka, A., Sebestova, E., Kozlikova, B., Brezovsky, J., Sochor, J., and Damborsky, J. (2016). CAVER: Algorithms for Analyzing Dynamics of Tunnels in Macromolecules. IEEE/ACM Trans Comput Biol Bioinform *13*, 505-517.
Pelosi, L., Ducluzeau, A.L., Loiseau, L., Barras, F., Schneider, D., Junier, I., and Pierrel, F. (2016). Evolution of Ubiquinone Biosynthesis: Multiple Proteobacterial Enzymes with Various Regioselectivities To Catalyze Three Contiguous Aromatic Hydroxylation Reactions. mSystems *1*, e00091-00016.
Poon, W.W., Davis, D.E., Ha, H.T., Jonassen, T., Rather, P.N., and Clarke, C.F. (2000). Identification of Escherichia coli ubiB, a gene required for the first monooxygenase step in ubiquinone biosynthesis. J. Bacteriol. *182*, 5139-5146.
Rea, S.L., Graham, B.H., Nakamaru-Ogiso, E., Kar, A., and Falk, M.J. (2010). Bacteria, yeast, worms, and flies: exploiting simple model organisms to investigate human mitochondrial diseases. Dev. Disabil. Res. Rev. *16*, 200-218.
Reidenbach, A.G., Kemmerer, Z.A., Aydin, D., Jochem, A., McDevitt, M.T., Hutchins, P.D., Stark, J.L., Stefely, J.A., Reddy, T., Hebert, A.S.*, et al.* (2017). Conserved Lipid and Small-Molecule Modulation of COQ8 Reveals Regulation of the Ancient Kinase-like UbiB Family. Cell Chem Biol.
Schoepp-Cothenet, B., van Lis, R., Atteia, A., Baymann, F., Capowiez, L., Ducluzeau, A.L., Duval, S., ten Brink, F., Russell, M.J., and Nitschke, W. (2013). On the universal core of bioenergetics. Biochim. Biophys. Acta *1827*, 79-93.
Sheldrick, G.M. (2015). Crystal structure refinement with SHELXL. Acta Crystallogr C Struct Chem *71*, 3-8.
Shestopalov, A.I., Bogachev, A.V., Murtazina, R.A., Viryasov, M.B., and Skulachev, V.P. (1997). Aeration-dependent changes in composition of the quinone pool in Escherichia coli - Evidence of post-transcriptional regulation of the quinone biosynthesis. FEBS Lett. *404*, 272-274.
Srere, P.A. (1985). THE METABOLON. Trends Biochem. Sci. *10*, 109-110.
Stefely, J.A., Licitra, F., Laredj, L., Reidenbach, A.G., Kemmerer, Z.A., Grangeray, A., Jaeg-Ehret, T., Minogue, C.E., Ulbrich, A., Hutchins, P.D.*, et al.* (2016). Cerebellar Ataxia and Coenzyme Q Deficiency through Loss of Unorthodox Kinase Activity. Mol. Cell *63*, 608-620.
Stefely, J.A., and Pagliarini, D.J. (2017). Biochemistry of Mitochondrial Coenzyme Q Biosynthesis. Trends Biochem. Sci. *42*, 824-843.
Su, G., Morris, J.H., Demchak, B., and Bader, G.D. (2014). Biological network exploration with Cytoscape 3. Curr Protoc Bioinformatics *47*, 8 13 11-24.
Winn, M.D., Ballard, C.C., Cowtan, K.D., Dodson, E.J., Emsley, P., Evans, P.R., Keegan, R.M., Krissinel, E.B., Leslie, A.G., McCoy, A.*, et al.* (2011). Overview of the CCP4 suite and current developments. Acta Crystallogr D Biol Crystallogr *67*, 235-242.

Wittig, I., Braun, H.P., and Schagger, H. (2006). Blue native PAGE. Nat. Protoc. *1*, 418-428.
Wollstein, C., Winterhalter, M., and Funari, S.S. (2015). The location of coenzyme Q10 in phospholipid membranes made of POPE: a small-angle synchrotron X-ray diffraction study. European Biophysics Journal with Biophysics Letters *44*, 373-381.
Wu, F., and Minteer, S. (2015). Krebs Cycle Metabolon: Structural Evidence of Substrate Channeling Revealed by Cross-Linking and Mass Spectrometry. Angewandte Chemie-International Edition *54*, 1851-1854.
Xia, H., Yang, X., Tang, Q., Ye, J., Wu, H., and Zhang, H. (2017). EsrE-A yigP Locus-Encoded Transcript-Is a 3' UTR sRNA Involved in the Respiratory Chain of E. coli. Front Microbiol *8*, 1658.
Yu, L.J., Suga, M., Wang-Otomo, Z.Y., and Shen, J.R. (2018). Structure of photosynthetic LH1-RC supercomplex at 1.9 A resolution. Nature *556*, 209-213.
Zhou, Z.H., McCarthy, D.B., O'Connor, C.M., Reed, L.J., and Stoops, J.K. (2001). The remarkable structural and functional organization of the eukaryotic pyruvate dehydrogenase complexes. Proc. Natl. Acad. Sci. U. S. A. *98*, 14802-14807.

Commented [FP1]: Insertion of one extra reference : Baba et al 2006 because the reference is cited in Table S5

Figure legends:

Figure 1: **UQ biosynthesis activity and Ubi proteins localize in the soluble fraction of *E. coli* extracts.** A) UQ biosynthesis pathway in *E. coli*. The octaprenyl tail is represented by R on the biosynthetic intermediates. Abbreviations used are DMAPP for dimethylallyl pyrophosphate, IPP for isopentenyl pyrophosphate, 4-HB for 4-hydroxybenzoic acid, $DDMQ_8$ for C2-demethyl-C6-demethoxy-ubiquinone 8, DMQ_8 for C6-demethoxy-ubiquinone 8 and UQ_8 for ubiquinone 8. B) Synthesis of $^{13}C_6$-UQ_8 from $^{13}C_6$-OPP accumulated in Δ*ubiC* cells. Cell free extracts, membrane and soluble fractions (resulting from 150.000g ultracentrifugation) were supplemented with NADH and SAM and incubated at 30°C in aerobic conditions for the indicated time. The area of the ^{13}C-UQ_8 peak (m/z 764.5 at a retention time of 8 min., see Figure S1E) was normalized for the protein content of the fractions assayed. Results representative of three independent experiments. C) Immunodetection of Ubi-SPA proteins (α-FLAG antibody) in soluble (s) and membrane (m) fractions of Ubi-SPA tagged strains (30 µg of total proteins) separated by SDS-PAGE. LamB and GAPDH are detected as controls. The ratio of the total content of each Ubi protein in entire soluble and membrane fractions is shown at the bottom (see Method Details). See also Figure S1.

Figure 2: **Seven Ubi proteins form a soluble Ubi complex.** A) BN-PAGE electrophoresis and immunodetection of soluble fractions from the indicated Ubi-SPA strains (50 µg of total proteins). The membrane was first probed with α-FLAG antibody, stripped and probed with α-GAPDH. B) Immunodetection with α-FLAG antibody of soluble fractions from the indicated Ubi-SPA strains after 1D BN-PAGE and 2D SDS-PAGE (50 µg of total proteins). C) SDS-PAGE and western-blot analysis (α-FLAG antibody) of fractions recovered from glycerol gradients onto which the cytoplasm of the indicated Ubi-SPA cells were deposited. A typical distribution of GAPDH is also shown. Fractions 1 and 22 correspond to the top and the bottom of the gradient, respectively (densities 1.02 and 1.11). Silver staining of gradient fractions analyzed by SDS-PAGE shows the distribution of total proteins (bottom). D) Separation by 1D BN-PAGE and 2D SDS-PAGE of glycerol gradient fractions 13-15 containing UbiG-SPA and immunodetection with α-FLAG antibody. The distribution of UbiG in all fractions of the gradient is shown (top). E) Interaction network between Ubi proteins constructed with Cytoscape 3 from the results of the bacterial two hybrid experiments (Table S1). Line width is proportional to the value of the interaction and cut off value was three times background. Interaction of proteins with themselves (for example UbiA-UbiA) are not represented. Results representative of two independent experiments (A-C). See also Figure S2.

Figure 3: **Purification of the Ubi complex.** A) Immunodetection with α-CBP antibody of the purified Ubi complex after 1D BN-PAGE and 2D SDS-PAGE (E2 fraction of UbiE-SPA, see Figure S2F). B) Silver staining of SDS-PAGE with purified E2 fractions from indicated -SPA samples and WT controls. Asterisks mark bands common to –SPA samples and absent from WT. C) Venn diagram integrating the different proteins found to be specifically enriched with each bait as compared with the related negative controls using MS-based proteomics (Table S2). The names of the eight proteins enriched with all three tagged Ubi proteins are indicated. See also Figure S2.

Figure 4: **The SCP2 domain of UbiJ binds UQ_8 and its biosynthetic intermediates in the Ubi complex.** A) Ratio of the abundance of octaprenyl lipids in the soluble fraction (SF, 150.000g supernatant) and the membrane fraction (MF) of WT cells grown in LB medium, mean ±SD (n=6). B) Glycerol gradient analysis of soluble extracts from UbiH-SPA cells and quantification of isoprenoid quinones in each fraction by HPLC-ECD-MS. Recovery calculated from the total content of all fractions compared to content of the UbiH-SPA soluble fraction deposited on top of the gradient. The western-blot showing the position of UbiH in the gradient is the same than in Figure 2C. C) Levels of OPP, DMQ_8 and UQ_8 in cells overexpressing or not UbiJ-K (n=4), see Figure S3C, **: p< 0.01, ***: p< 0.001, unpaired Student's t test. D) Abundance of isoprenoid quinones in the indicated purified proteins (see Figure S3E), mean ±SEM (n=2). See also Figure S3.

Figure 5. Structure of UbiJ-SCP2 at 1.7 Å resolution. A) UbiJ-SCP2 appearing as a dimer within the asymetric unit, monomers contain a beta sheet consisting of 5 strands and 5 alpha helices similar to SCP2 family proteins (chain A in orange, chain B in teal). B) Yellow spheres represent the cavity found in UbiJ-SCP2 (cavity modelled using CAVER3 plugin for Pymol). C) Model of the cavity area of UbiJ-SCP2 with the hydrophobic residues lining the cavity highlighted in yellow and showing unmodelled electron density (maps for 2FoFc are set at 1 σ [blue mesh]and for FoFc are set at 3 σ [green mesh]). D) Sequence for UbiJ-SCP2 with hydrophobic residues interfacing with the cavity pocket shown in yellow (cylinders represent α-helices, arrows β-strands). E) Hydrophobic cavities in UbiJ-SCP2 chain A (top) and chain B (middle), and comparison with ubiquinone 8 (bottom, taken from PDB: 5Y5S). The respective lengths are indicated. See also Figure S4 and S5.

Figure 6: **UbiJ is essential to the stability of the Ubi complex.** A) Glycerol gradient analysis of soluble extracts from UbiG-SPA *ΔubiJ* cells and quantification of UQ_8 and OPP in each fraction. Western-blots show the distribution of UbiG-SPA and the control GAPDH protein (see also Figure S6C-D, recovery calculated as in Figure 4B). B-C) Immunodetection with α-FLAG antibody of soluble fractions from the UbiH-SPA strain carrying deletions in the indicated *ubi* genes after BN-PAGE analysis (B) or 1D BN-PAGE and 2D SDS-PAGE (C). D-E) Immunodetection with α-FLAG antibody of soluble fractions from the indicated Ubi-SPA strain carrying deletions for *ΔubiJ* (D) or *ΔubiK* (E) after 1D BN-PAGE and 2D SDS-PAGE. A representative result from 2 independent experiments is shown (B-E). F) UQ_8 biosynthetic pathway (top) and proposed model of the physical organization of Ubi proteins and prenylated UQ_8 intermediates with respect to the inner membrane. The same representation is used for all polyprenylated compounds, irrespective of the substituents of the benzoquinone head group. Membrane-bound UbiA prenylates 4HB to yield OHB that localizes in the lipid bilayer. UbiB assists the extraction of OHB from the membrane and OHB is subsequently decarboxylated to OPP by UbiD-X. OPP is bound by UbiJ in the Ubi complex and the metabolon formed by the seven Ubi proteins circled in red synthesizes UQ_8, which is ultimately delivered to the membrane, where it fulfills its physiological functions. See also Figure S6.

606 ## STAR Methods

607 **CONTACT FOR REAGENT AND RESOURCE SHARING**

608 Further information and requests for resources and reagents should be directed to and will be
609 fulfilled by the Lead Contact, Fabien Pierrel (fabien.pierrel@univ-grenoble-alpes.fr)

610 **EXPERIMENTAL MODEL AND SUBJECT DETAILS**

611 *E. coli* strains were stored frozen at -80°C in solutions containing 20% glycerol and revived by streaking
612 on LB plates containing 1.6% bacto-agar (w/v) and incubating overnight at 37°C. Plates were kept at
613 4°C for up to three weeks and colonies from the plates were used to inoculate overnight precultures
614 in liquid medium. Large cultures were performed by inoculating fresh growth medium at O_{D600} 0.05
615 with the precultures. *E. coli* strains were grown in lysogeny broth (LB) medium at 37 °C in Erlenmeyer
616 flasks filled to 1/10 of the maximal volume and shaken at 180 rpm, unless stated otherwise. For
617 experiments using labelling with $^{13}C_7$-4-HB, cells were grown in MSG medium, a minimal medium
618 supplemented with 0.4% glycerol (w/v) (Alberge et al., 2015). All growth media were sterilized by
619 autoclave and then ampicillin (50 mg/L), kanamycin (25 mg/L), and chloramphenicol (25 mg/L) were
620 added from stocks (1000X solution sterilized through 0.22 µm filters and stored at -20°C), when
621 needed. MSG medium was supplemented with 0.5% casaminoacids (w/v) and with 1/100 volume of a
622 filter-sterile solution of 1mM $CaCl_2$, 200 mM $MgCl_2$, 1% thiamine (w/v).

623 **METHOD DETAILS**

624 ***Strain construction*:**
625 All strains used in this study are listed in Table S5.
626 Construction of SPA strains:
627 The DY330 *ubiC-SPA* strain encompassing the SPA tag DNA sequence and the kanamycin antibiotic
628 resistance marker cassette (Kan^R) was used as a template in polymerase chain reaction (PCR)
629 amplification. A 5-*ubiD, E, I, J, K* -SPA gene-specific forward primer (Table S6), located immediately

upstream of the *ubi* stop codon, and a 3-*ubiD, E, I, J, K* -SPA gene-specific reverse primer, located immediately downstream of the target gene stop codon, were used to amplify the SPA tag and Kan^R cassette. The purified PCR products were subsequently integrated at the 3′ end of *ubi* genes or atpB gene in the BW25113 strain in which the λ-Red recombination machinery is expressed. Finally, the *ubi*–SPA–Kan cassettes were transduced through P1 phage from BW25113 to MG1655. When DY330 SPA-tagged strains were available (Hu et al., 2009), the *ubi*–SPA–Kan cassettes were transduced to MG1655 through P1 phage.

Construction of knock-out strains:

The *ubiC*::Kan, *ubiE*::Kan, *ubiF*::Kan, *ubiG*::Kan mutations (from the BW25113 strains, Keio library) and *ubiJ*::Kan, *ubiK*::Kan mutations were transduced into the desired MG1655 strain by P1 transduction.

Plasmid construction:

The two-hybrid plasmids were constructed by inserting the *ubi* ORF sequences in pT18 and pT25 plasmids, using the oligonucleotides indicated in Table S6. Briefly, the *ubi* gene fragments were obtained by PCR amplification using the genomic DNA of MG1655 as template and the oligonucleotides 5-*Xha*I *ubi and* 3-*Xba*I *ubi*. PCR products were *Xba*I-digested and inserted into *Xba*I-digested pT18 or pT25 plasmids, yielding the pT18-ubi and pT25-ubi plasmids, respectively. All plasmids were verified using DNA sequencing.

Bacterial two-hybrid reporter system:

The bacterial two-hybrid reporter system is based on functional complementation of the two domains of *Bordetella pertussis* adenylate cyclase, T18 and T25, expressed separately from two compatible plasmids (Karimova et al., 1998). Adenylate cyclase activity is restored only when proteins fused to T18 and T25 interact. Fusions were constructed with T18 and T25 present at the N-terminal of Ubi proteins. Functional reconstitution of *B. pertussis* adenylate cyclase in an *E. coli* _*cya lac*_ strain was monitored by assaying the activity of a cAMP-CRP-dependent lac promoter of a chromosomally encoded lac

operon. In addition to testing the pair of proteins of interest, positive controls were performed with T25-zip and T18-zip plasmids. Negative controls were performed with the two empty T18 and T25 plasmids and also with each protein of interest against the empty T18 or T25 plasmids.

The interaction network of Ubi proteins in Figure 1E was constructed with Cytoscape 3 (Su et al., 2014) from the results of the bacterial two hybrid experiments (Table S1), excluding values less than 3 times above background.

Preparation of soluble and membrane fractions:

Ubi-SPA strains were cultured in 1 L of LB medium (2 L flasks) with shaking (200 rpm) at 37°C. When OD_{600} reached 1.5-2, cells were cooled down on ice with occasional shaking and harvested by centrifugation at 5,000 g for 20 min at 4°C. The cell pellet was washed with 10 mL cold water, the same centrifugation was repeated and the pellet was frozen in liquid nitrogen, then stored at -80°C. The cell pellet was resuspended in 30 mL buffer A (50 mM Imidazole/HCl pH=7, 50 mM NaCl, 1 mM EDTA, 1 mM PMSF, 250 mM sucrose; (adapted from (Wittig et al., 2006))) and the cells were ruptured by 3 passages through French press (1,500 psi). Cell debris were eliminated by centrifugation at 3,200 g for 10 min at 4°C, then 20 mL of the supernatant was subjected to ultracentrifugation at 120,000 g for 1h at 4°C. The supernatant after ultracentrifugation corresponds to the soluble fraction. The pellet was resuspended in 2 mL of buffer A to yield the membrane fraction. Aliquots of both fractions were frozen with liquid nitrogen and stored at -80°C.

Protein concentration and SDS-PAGE:

Protein concentrations were determined by the bicinchoninic acid assay (Thermo). 30 µg of total protein were analyzed on 12% acrylamide SDS-PAGE gel and electrophoresis was performed at 20 mA for 45 min. Prestained Protein Ladder (Euromedex) was used as molecular weight marker.

Blue Native-PAGE:

Native PAGE sample additive (Life Technologies) was added to the soluble fractions (50 µg of proteins) and BN-PAGE was performed using Native PAGE 3–12% Bis–Tris gels (1.0 mm × 10 wells; Life

680 Technologies). The BN-PAGE system consisted of two compartments: the internal one contained the
681 cathode buffer (50 mM tricine, 7.5 mM imidazole, 0.02% coomasie blue G250, pH=7) whereas the
682 external one contained the NativePAGE running buffer (50 mM Bis–Tris pH=7, 50 mM tricine, Life
683 Technologies). Electrophoresis was performed at 4°C using 3 tensions: 100V for 20 min allowing
684 proteins to enter the gel, 200V for 30 min then 300V until the migration front reached the lower limit
685 of the gel (~1h). Proteins were transferred onto an immobilon PVDF membrane pre-activated for 2 min
686 with methanol. Transfer was performed in buffer B (50 mM Tricine, 7.5 mM imidazole, pH=7) for 3h at
687 4°C with 20 mV tension. At the end of the transfer, the PVDF membrane was discolored by rinsing
688 several times with a mixture of 20% methanol and 10% acetic acid in order to visualize the molecular
689 weight marker (NativeMark, Life Technologies). The position of marker bands on the membrane was
690 marked with pencil and full discoloration of the membrane was obtained with 100% methanol. The
691 membrane was further processed for western-blotting.

692 ***Two dimensional BN-PAGE/SDS-PAGE:***

693 After the BN-PAGE was completed, gel lanes were cut out of the gel, soaked in SDS-PAGE running
694 buffer (0.375 M Tris-HCl, pH 8.8, glycine 0.192 M, SDS 10%) for 15 min and then loaded onto a 12.5%
695 acrylamide SDS gel of 1.5 mm thickness. 5 µL of molecular weight marker (prestained protein ladder)
696 was deposited on a Whatman paper, which was positioned next to the BN-PAGE fragment. BN gel and
697 SDS gel were glued together using buffer C (0.5% agarose dissolved in SDS running buffer and few
698 drops of 0.5% bromophenol blue). Migration was performed at 20 mA until the migration front reached
699 the bottom of the gel. Transfer was performed using trans-blot turbo system (Bio-Rad) 17 V, 10 min.

700 ***Western-blot analyses:***

701 After transfer, membranes were saturated with 5% milk in PBST (Phosphate-buffered saline, 0.2%
702 Tween-20) for 30 min, rinsed 3 times in PBST and incubated overnight with the primary antibody in
703 PBST at 4°C on a rotary table. Primary antibodies were used at the following dilutions: α-FLAG antibody,
704 1/5000; α-CBP, 1/3000; α-GAPDH, 1/5000; α-LamB, 1/3000. Immunodetection was performed using
705 goat anti-rabbit HRP-conjugated or goat anti-mouse HRP-conjugated and the Clarity Western ECL

substrate (BioRad). Images were acquired on a ChemiDoc XRS system with the Image Lab software (BioRad). When detection with a second antibody was needed, the membrane was stripped by three successive incubations in stripping buffer (glycine-HCl 1.5% (m/V) pH 2.2, SDS 0.1% (m/V), Tween 1% (V/V)), then rinsed in PBST and saturated with 5% milk in PBST.

The s/m ratio in Figure 1C were calculated as follows. The intensity of each protein band (quantified from the western-blot with Image Lab software) was multiplied by the total protein content of the corresponding fraction (typically, 18 mL at ~5 mg protein/mL for FS and 2 mL at ~19 mg protein/mL for FM) to estimate the total content of Ubi-SPA proteins in s and m fractions. Then, we computed the quotient of the values obtained for s and m for each Ubi-SPA protein.

Silver staining:

The SDS-gel was placed in fixing solution (50% methanol, 5% acetic acid) and agitated gently on a rotary shaker for 20 min. The gel was then rinsed in 50% methanol for 10 min, in water for 10 min and was agitated gently in 100 mL of 0.02% sodium-thiosulfate for 1 min, followed by two washing steps with water for 1 min. The gel was incubated for 20 min in 200 mL of 0.2% silver nitrate solution supplemented with 0.08% formaldehyde. The gel was washed with distilled water for 20 sec to remove the excess silver nitrate and was then placed in 50 mL of developing solution (2% sodium carbonate and 0.04% formaldehyde). When the desired intensity was obtained, the gel was transferred to 5% acetic acid for 20 min to stop the reaction. After rinsing with distilled water for 10 min, the gel was stored in 5% glycerol.

Overexpression and purification of proteins:

The UbiJ(6his)-UbiK and UbiK proteins were overexpressed and purified as previously described (Loiseau et al., 2017). Overexpression of UbiJ-SCP2 was performed in BL21 (DE3) *E.coli* strain transformed with the previously reported pETDuet-ubiJ(Δ121–201) (Loiseau et al., 2017). Cells were grown with shaking (200 rpm) at 37°C, in lysogeny broth (LB) medium containing ampicillin (100 µg/ml), until they reached OD_{600} = 0.4, at which point overexpression was induced by addition of

lactose (5.8 mM). After induction, cells were grown for 17 hours at 16°C, and then harvested by centrifugation at 5,000 g for 10 min. All subsequent operations were carried out at 4°C. Cells were resuspended in 5 volumes of buffer D (50 mM Tris-HCl pH 7.5, 150 mM NaCl, 1 mM phenylmethylsulfonyl fluoride) and lyzed by sonication (Branson Digital Sonifier, Amplitude 40% for 10 min). Crude extracts were then submitted to ultracentrifugation at 180,000 g for 90 min (Optima XPN-80, rotor 50.2 Ti, Beckman Coulter). The resulting supernatant was loaded onto a Hitrap Chelating HP column (5 mL, GE Healthcare) equilibrated with buffer D. The Hitrap Chelating HP column was washed with buffer D supplemented with 25 mM imidazole and subsequently eluted with 300 mM imidazole in buffer D. The most pure UbiJ-SCP2 fractions were pooled and loaded onto a HiLoad 26/600 Superdex 75 pg equilibrated with 50 mM Tris-HCl pH7.5, 150 mM NaCl. The main peak fractions were pooled, frozen in liquid N2 and stored at - 80°C.

Crystallization:

Crystals were grown at 19 °C by the hanging drop vapor diffusion method. Initial reservoir crystallization hit consisted of 18% PEG 8000, 200 mM calcium acetate hydrate with 100 mM sodium cacodylate trihydrate pH 6.5. Crystal growth was observed in high protein concentration of no less than 15 mg/mL. The reservoir condition was optimized for best crystal growth to consist of 11% PEG 8000, 225 mM calcium chloride with 100 mM MMT buffer pH 9 (MMT is DL-malic acid/MES/Tris base mixed at a ratio of 1/2/2 and pH-adjusted with sodium hydroxide). Rod-like crystals grew within the precipitate overnight. All crystals were cryoprotected in a solution similar to the reservoir solution containing 20 % PEG 400 prior to flash freezing. Best diffraction of these crystals led to the initial 2.5 Å dataset (PDB code 6H6P). Derivatisation of these crystals led to lower resolution diffraction and poor anomalous signal. These crystals were used for seeding which led to more consistent crystal shape however after these conditions had been left for over a month a more cubic shaped crystal form appeared in the condition. This new crystal form diffracted to 1.7 Å (PDB code 6H6O) and when used for seeding resulted in cubic crystal growth at a much lower protein concentration of 2.5 mg/ml. These

crystals natively diffracted well and were used for derivatisation using various heavy atom compounds. Polyvalan crystallophore No1 was used in cocrystallisation and resulted in crystals diffracting to 2 Å with significant anomalous signal allowing phasing of the data for structure determination (PDB code 6H6N).

***Data collection and structure determination*:**

All crystals belong to the space group P212121. The 2.5 Å dataset has a unit cell parameters of a= 47.69 Å; b= 94.55 Å; c= 115.66 Å, and four molecules per asymmetric unit. The 1.7 Å has a unit cell parameters of a= 48.6 Å; b= 67.87 Å; c= 74.60 Å, and the 2.05 Å dataset has a unit cell parameters of a= 48.30 Å; b= 67.93 Å; c= 73.08 Å, and both have two molecules per asymmetric unit. The 2.5 Å X-ray diffraction data were collected from single crystal at 100 K on the EIGER X 9M detector on beamline Proxima 2 at the Soleil synchrotron radiation source, Paris. The 1.7 Å and 2.05 Å X-ray diffraction data were collected from single crystals at 100 K on the Pilatus detector on beamline Proxima 1 at the Soleil synchrotron radiation source, Paris. Data were processed and scaled using the package XDS (Kabsch, 2010). Anisotropy and diffraction limits were set using the program STARANISO (Bricogne et al., 2017). Phases were obtained from 2 Terbium sites in the 2.05 Å dataset using SHELX (Sheldrick, 2015). Model was automatically built using Buccaneer and further manual building using the program Coot (Cowtan, 2006; Emsley et al., 2010) with refinement performed using BUSTER (Bricogne et al., 2017). This model was then used to molecular replace the two other datasets for their further modelling and refinement using the same methods. The CCP4 software suite was also used in processing of data and Pymol was used in production of images including the CAVER3 plugin for cavities (Chovancova et al., 2012; Pavelka et al., 2016; Winn et al., 2011).

***$^{13}C_6$-UQ_8 biosynthesis activity assay*:**

Δ*ubiC* cells from an overnight preculture were inoculated at OD_{600} 0.15 in 100 mL MSG medium. The cells were cultured at 37°C, 200 rpm until OD_{600} 1, at which point chloramphenicol (200 µg/mL) was

781 added and incubation continued for 20 min. Then, the cells were transferred to a screw cap flask fitted
782 with two plastic tubing through which the culture was purge with argon for 5 min. 10 µM $^{13}C_7$-4-HB
783 was added, the cells were maintained under argon at 37°C and initial experiments following the
784 biosynthesis of $^{13}C_6$-OPP at different incubation time established that 10 min labeling with $^{13}C_7$-4-HB
785 was optimal (Figure S1B). Cells were cooled down on ice under argon. In all subsequent steps carried
786 out under normal atmosphere, care was taken to maintain the cells at 4°C in order to avoid conversion
787 of $^{13}C_6$-OPP into $^{13}C_6$-UQ_8. Cold cells were collected by centrifugation at 3,200 g, 4°C, 10 min and
788 resuspended in 10 mL cold standard buffer (50 mM Tricine pH 7.5, 5 mM $MgSO_4$, 10 mM β-
789 mercaptoethanol).

790 For the *in vivo* assay, the cells were diluted five-fold in MSG medium containing 200 µg/mL
791 chloramphenicol and incubated at 37°C either in normal atmosphere with 180 rpm shaking or under
792 argon, a condition in which $^{13}C_6$-UQ_8 did not form. For the *in vitro* assay, cells in standard buffer were
793 ruptured by 3 passages through French press (1500 psi) and debris were eliminated by centrifugation
794 at 8,000 g for 20 min at 4°C. The cell free lysate was either directly assayed by adding 2 mM NADH, 2
795 mM SAM and incubating at 30°C with occasional shaking or ultracentrifuged at 150,000 g, 4°C for 90
796 min. The supernatant corresponding to the soluble fraction was taken and the membrane pellet was
797 resuspended in a volume of standard buffer equal to that of the supernatant. 300 µL fractions were
798 assayed by adding 2 mM NADH and 2 mM SAM and incubating at 30°C with occasional shaking. The
799 reactions were stopped by placing the samples at -20°C prior to lipid extraction and HPLC-ECD-MS
800 analysis.

801 ***Lipid extraction and quinone analysis*:**

802 Quinone extraction from cell pellets and quantification by HPLC-ECD-MS analyses were performed as
803 previously described (Loiseau et al., 2017). Aliquots of glycerol gradient fractions (250 µL) or of
804 membrane (100 µL) and soluble fractions (400 µL) were extracted twice in glass tubes with 3 mL
805 methanol, 30 µL KCl 3M and 2*2 mL p-ether. Depending on the separation needed, mobile phase 1

(40% ethanol, 40% acetonitrile and 20% of a mix of 90% isopropanol, 10% ammonium acetate (1 M), 0.1% TFA) or mobile phase 2 (50% methanol, 40% ethanol and 10% of a mix of 90% isopropanol, 10% ammonium acetate (1 M), 0.1% TFA) were used at a flow rate of 1 mL/min with a BetaBasic-18 column. MS detection was on a MSQ spectrometer (Thermo Scientific) and electrospray ionization in positive mode used a probe temperature of 400°C and a cone voltage of 80V. Single ion monitoring (SIM) detected the following compounds: OPP ($M+NH_4^+$), m/z 656.0-656.8, 5-10 min, scan time 0.2 s; $^{13}C_6$-OPP ($M+ NH_4^+$), m/z 662.0-662.8, 5-10 min, scan time 0.2 s; DMQ_8 ($M+NH_4^+$), m/z 714.0-714.8, 6-10 min, scan time 0.2 s; UQ_8 ($M+NH_4^+$), m/z 744.0-744.8, 6-10 min, scan time 0.2 s; $^{13}C_6$-UQ_8 ($M+Na^+$), m/z 755.0-755.8, 6-10 min, scan time 0.3 s; UQ_{10} ($M+NH_4^+$), m/z 880.2-881.2, 10-17 min, scan time 0.2 s. For some analyses, 0.1mM methylamine was added to the methanol of mobile phase 2, in which case the probe temperature was 450°C and SIMs were set as follows: UQ_8 ($M+CH_3NH_3^+$), m/z 758.0-758.8, 6-10 min, scan time 0.2 s; $^{13}C_6$-UQ_8 ($M+CH_3NH_3^+$), m/z 764.0-764.8, 6-10 min, scan time 0.3 s; UQ_{10} ($M+CH_3NH_3^+$), m/z 894.2-895.2, 10-17 min, scan time 0.2 s. MS spectra were recorded between m/z 600 and 900 with a scan time of 0.3 s. UV detection at 247 nm was used to quantify DMK_8 and MK_8. Peak areas were corrected for sample loss during extraction on the basis of the recovery of the UQ_{10} internal standard and were then normalized either to cell's wet weight, or to total proteins (soluble and membrane fractions), or to quantity of purified protein, or to the total content of the fraction deposited on glycerol gradients. The peak of UQ_8 obtained with electrochemical detection was quantified with a standard curve of UQ_{10} (Hajj Chehade et al., 2013).

Purification of the Ubi complex:

Ubi-SPA and WT strains were cultured in 1 L LB medium (2 L flasks) with shaking (200 rpm) at 37°C until OD_{600} = 2.5-3. Soluble fractions were prepared in 10 mL lysis buffer (10 mM Tris-HCl pH 7.9, 100 mM NaCl, 10 mM DTT) with 1X anti-protease (sigma*FAST* protease inhibitor). The subsequent two steps purification procedure was carried out at 4°C with ice cold buffers and we indicate below the names of the fractions analyzed in Figure S2c-g. 100 µL of anti-Flag M2 agarose beads (Sigma) were first washed with 10 mL lysis buffer (without DTT) and the beads were added to the ultracentrifugation

supernatant in a 15 mL Falcon tube. The mixture was rotated moderately (20 rpm) for 3h, then transferred to a 10 mL disposable chromatography column (EconoPac, BioRad) and the unbound material was eluted by gravity (FT-FLAG). The resin was washed with 30 mL lysis buffer (W1) followed by 30 mL TEV cleavage buffer (50 mM Tris-HCl pH 7.9, 100 mM NaCl and 0.2 mM EDTA) (W2). The 3X FLAG motif was cleaved by adding 500 µL of TEV cleavage buffer containing 1X anti-protease, 1 mM DTT and 50 µg Tobacco Etch Virus protease (TEV) and by incubating overnight under rotation. The next day, the eluate was drained into a fresh Eppendorf tube (El-TEV).

Prior to use, 100 µL of Calmodulin-Sepharose 4B beads were transferred into a 15 mL tube (Falcon), washed twice in batch with 10 mL of CBP binding buffer (10 mM Tris-HCl pH 7.9, 100 mM NaCl and 2 mM $CaCl_2$) and the beads were suspended in 500 µL of TEV cleavage buffer containing 2 mM $CaCl_2$ and 10 mM β -mercaptoethanol. The beads suspension was added to the eluate recovered after TEV cleavage and the mixture was rotated for 3h in an Eppendorf tube. The sample was transferred to a 1.5 mL chromatography column (Mini-columns, Evergreen Scientific) and the unbound fraction was drained by gravity (FT-CBP). The beads were then washed 5 times with 500 µL of calmodulin washing buffer (10 mM Tris-HCl pH 7.9, 100 mM NaCl, 1 mM $CaCl_2$, 10 mM β-mercaptoethanol) (W1-W5). The bound proteins were eluted in five fractions of 100 µL using the calmodulin elution buffer (10 mM Tris-HCl pH 7.9, 200 mM NaCl, 3 mM EGTA, 10 mM β-mercaptoethanol) (E1-E5).

***Glycerol gradient fractionation*:**

1 mL soluble fractions of Ubi-SPA strains were deposited on 10 mL linear glycerol gradients prepared using two glycerol solutions (densities 1.025 and 1.110) in modified buffer A (50 mM Imidazole/HCl pH=7, 50 mM NaCl, 1 mM EDTA). Fractions of 0.5 mL were collected manually from the bottom of the tubes after centrifugation for 15h at 120,000 g and 4°C in a swinging bucket rotor (Beckman SW-41). 15 µL of each fraction were analyzed by SDS-PAGE, SPA-tagged proteins were immunodetected and the reproducibility of the gradients was verified by immunodetection of GAPDH. Quinone quantification in glycerol gradient fractions was measured from 200 µL aliquots.

***Mass spectrometry-based proteomic analyses*:**

Proteins were in-gel digested using trypsin as described in (Barral et al., 2017). The resulting peptides were analyzed by online nano-liquid chromatography coupled to tandem mass spectrometry (Ultimate 3000 nano RSLC and Q-Exactive HF, Thermo Scientific) using a 120-min gradient. Peptides were sampled on a 300 µm x 5 mm PepMap C18 precolumn (Thermo Scientific) and separated on a 75 µm x 250 mm C18 column (Reprosil-Pur 120 C18-AQ, 1.9 µm, Dr. Maisch). MS and MS/MS data were acquired using Xcalibur (Thermo Scientific). Peptides and proteins were identified using Mascot (version 2.6.0) through concomitant searches against Uniprot (Escherichia coli K12 taxonomy), classical contaminants database (homemade) and the corresponding reversed databases. The Proline software (http://proline.profiproteomics.fr) was used to filter the results (conservation of rank 1 peptides, peptide identification FDR < 1% as calculated on peptide scores by employing the reverse database strategy, minimum peptide score of 25, and minimum of 1 specific peptide per identified protein group) before performing a compilation, grouping and comparison of the protein groups from the different samples. Proteins were considered as potential partners of the bait if they were identified only in the positive co-IPs with a minimum of 5 specific spectral counts or enriched at least 10 times in positive co-IPs compared to control ones on the basis of specific spectral counts.

QUANTIFICATION AND STATISTICAL ANALYSIS

See each individual method and figure legends for the associated statistical analysis. In general, p-values were calculated using an unpaired, two-tailed, Student's t-test. In all cases, n represents independent replicates of an experiment.

DATA AND SOFTWARE AVAILABILITY

The mass spectrometry proteomics data have been deposited to the ProteomeXchange Consortium via the PRIDE partner repository with the dataset identifier PXD010396.

882 The crystal structures of the SCP2 domain of UbiJ have been deposited in the Protein Data Bank PDB
883 with the identifiers 6H6N, 6H6O and 6H6P.

884 Supplemental Information

885 Supplemental information contains 6 supplemental figures and 6 supplemental tables.

Figure 1

Click here to access/download;Figure;fig1.tif

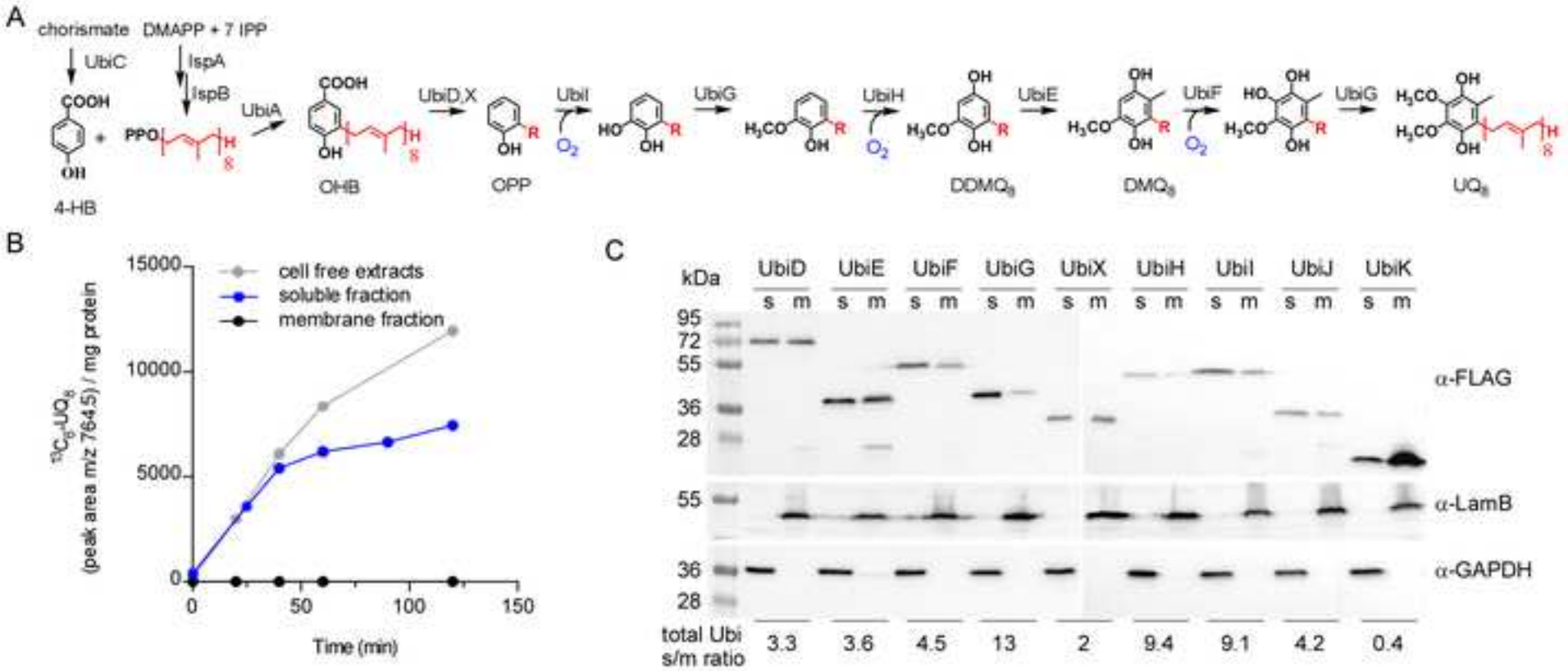

Figure 5

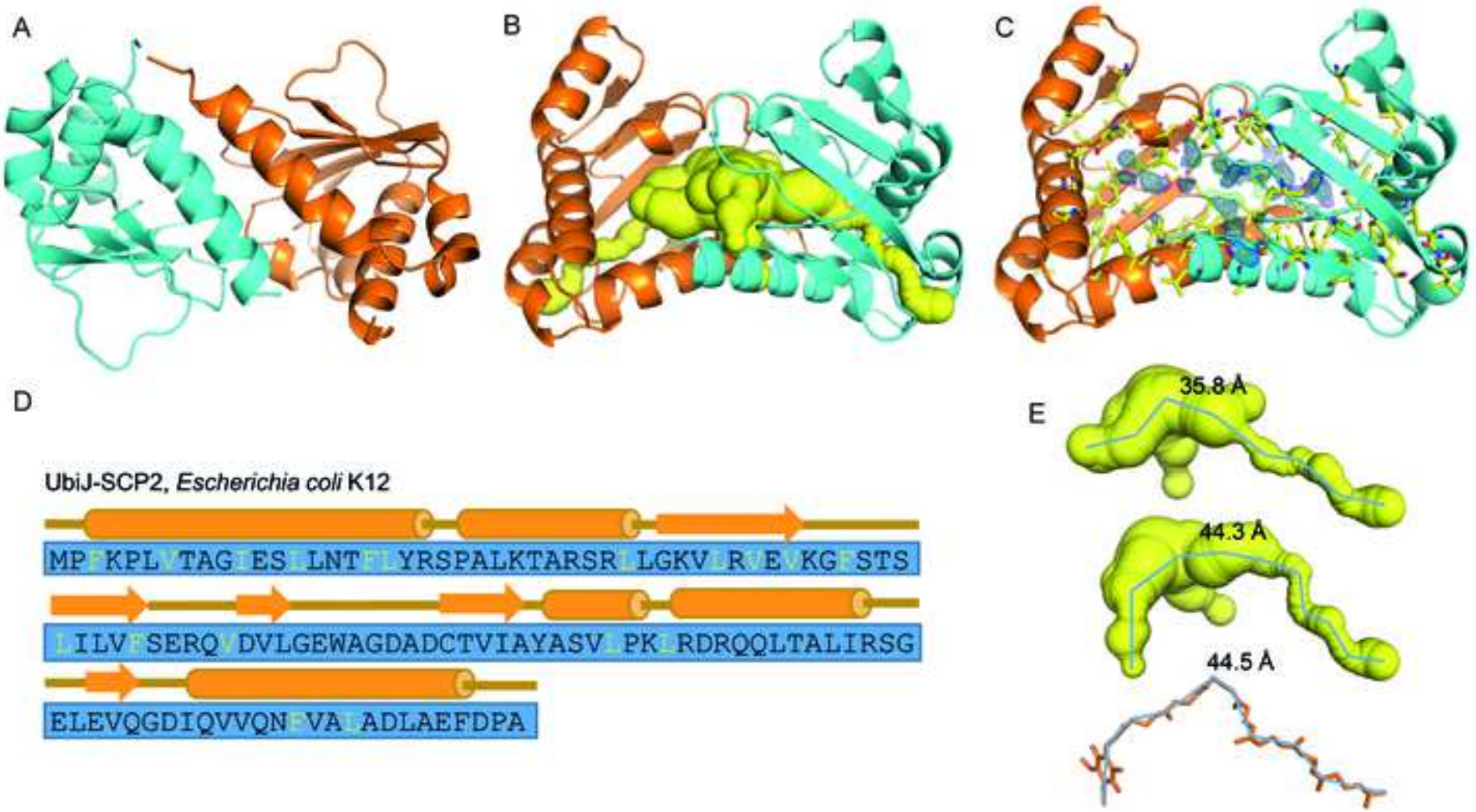

Figure 6

Click here to access/download;Figure;fig 6.tif

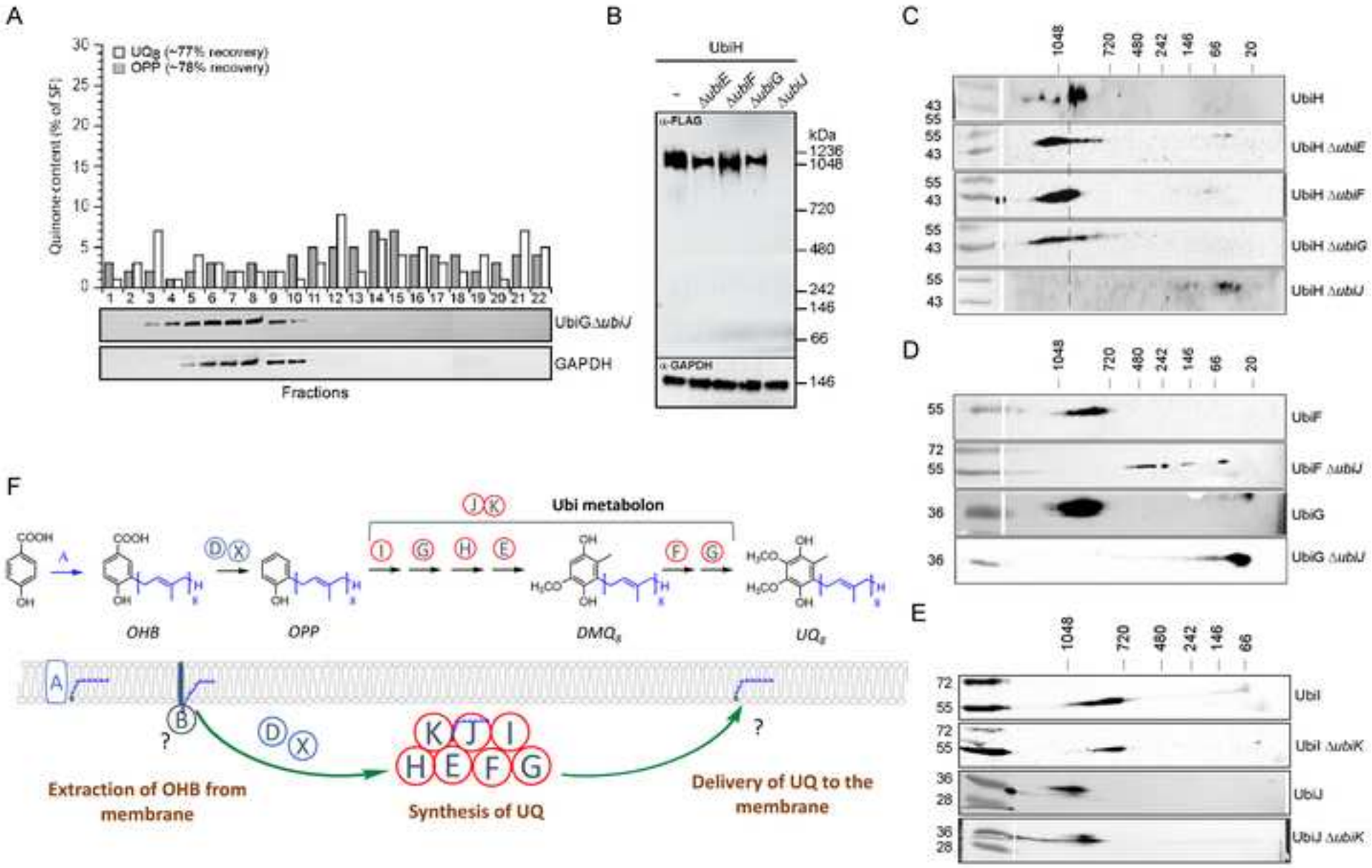

Figure 2

Click here to access/download;Figure;fig 2.tif

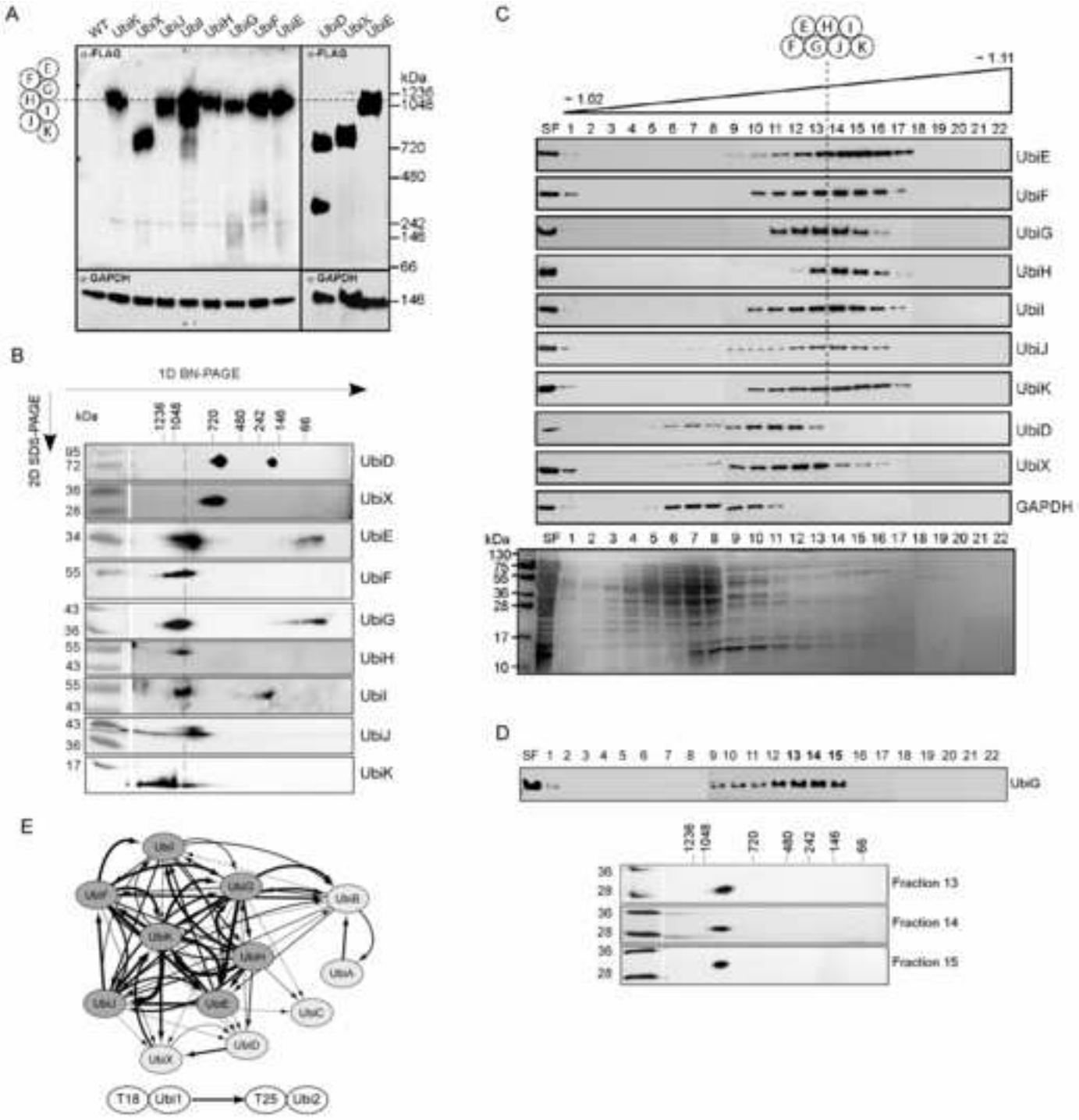

Figure 3

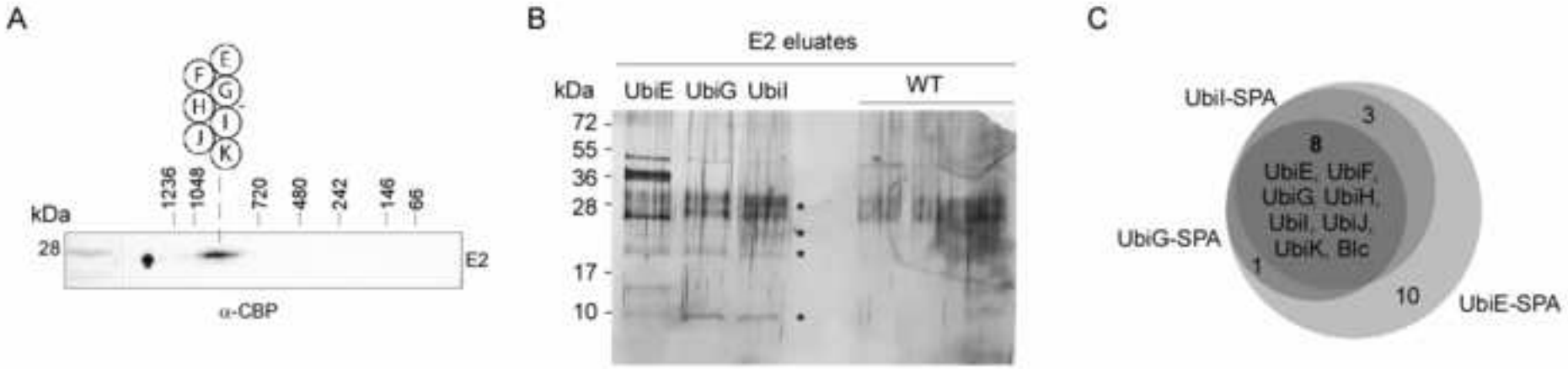

Figure 4

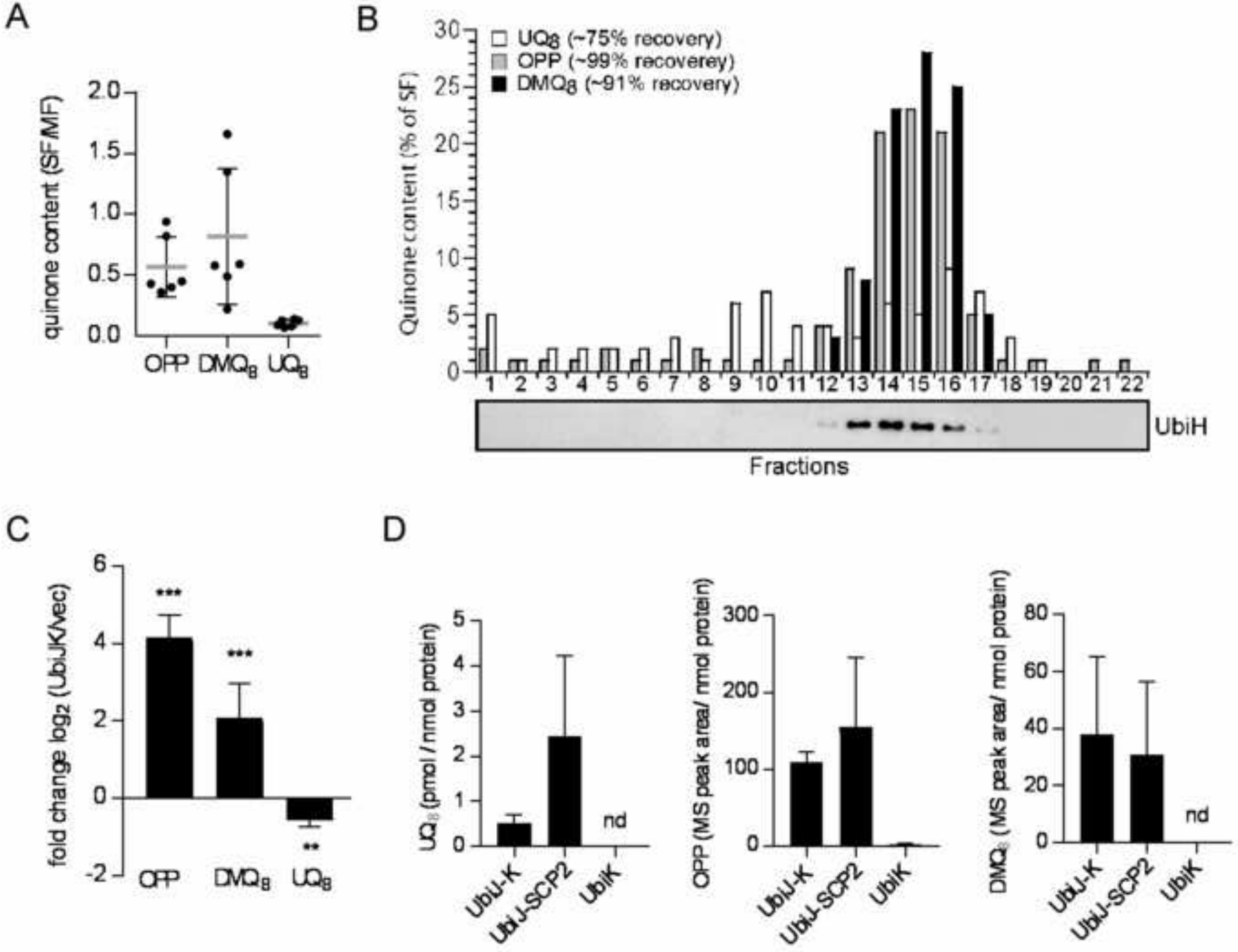

KEY RESOURCES TABLE

REAGENT or RESOURCE	SOURCE	IDENTIFIER
Antibodies		
α-FLAG	Sigma Aldrich	Cat# A2220 (RRID:AB_10063035)
α-Calmodulin Binding Peptide	Genscript	Cat# A00635-40 (RRID:AB_914284)
α-GAPDH	Covalab	Cat# 00006357
α-LamB	A. Meinke, Intercell AG	N/A
goat anti-rabbit HRP-conjugated	Covalab	Cat# 00030130
goat anti-mouse HRP-conjugated	Covalab	Cat# 00030133
Bacterial and Virus Strains		
E. coli MG1655	ATCC	ATCC 47076
E. coli BW25113	National BioResource Project	http://nbrp.jp/ search for ME9062
E. coli BL21 (DE3)	Merck Millipore	Cat# 69450-3
E. coli BTH101	(Karimova et al., 1998)	N/A
E. coli DY330	(Hu et al., 2009)	N/A
Biological Samples		
Chemicals, Peptides, and Recombinant Proteins		
$^{13}C_7$-4-HB	Sigma Aldrich	Cat# 587869
NADH	Sigma Aldrich	Cat# 43420
S-Adenosylmethionine	Sigma Aldrich	Cat# A2408
anti-Flag M2 agarose beads	Sigma Aldrich	Cat# A2220
Calmodulin-Sepharose 4B beads	Sigma Aldrich	Cat# GE17-0529-01
sigmaFAST protease inhibitor	Sigma Aldrich	Cat# S8830
Prestained (Two Colors) Protein Ladder Plus (10-250Kda)	Euromedex	Cat# 06P-0211
Native PAGE sample additive	Life Technologies	Cat# BN2003
Native PAGE 3–12% Bis–Tris gels	Life Technologies	Cat# BN1001BOX
Native PAGE 20X Running Buffer	Life Technologies	Cat# BN2001
NativeMark protein ladder	Life Technologies	Cat# LC0725
Polyvalan crystallophore No1	Molecular Dimensions	Cat# MD2-81
Purified UbiK protein	This study	N/A
Purified UbiJ-SCP2 protein	This study	N/A
Purified UbiJ-K complex	This study	N/A
Sequencing Grade Modified Trypsin	Promega	V5111
Dithiothreitol	Fisher Scientific	BP172
Iodoacetamide	Sigma Aldrich	I1149
Ammonium bicarbonate	Sigma Aldrich	A6141
Formic acid	EMD Millipore Chemical	1.11670.0250
Acetonitrile	Sigma Aldrich	34851-M

Critical Commercial Assays		
Deposited Data		
mass spectrometry proteomics data	This study	http://www.proteomexchange.org PXD010396
X-ray structure of UbiJ-SCP2, 2.1 Å	This study	http://www.rcsb.org/ PDB ID: 6H6N
X-ray structure of UbiJ-SCP2, 1.7 Å	This study	PDB ID: 6H6O
X-ray structure of UbiJ-SCP2, 2.5 Å	This study	PDB ID: 6H6P
Experimental Models: Cell Lines		
Experimental Models: Organisms/Strains		
For all *E. coli* strains, see Table S5		
Oligonucleotides		
For all primers, see Table S6	This paper	N/A
Recombinant DNA		
pETDuet-6his-ubiJ/ubiK	(Loiseau et al., 2017)	N/A
pETDuet-ubiJ(Δ121–201)	(Loiseau et al., 2017)	N/A
pETDuet-ubiK no-tag	(Loiseau et al., 2017)	N/A
pT18	(Karimova et al., 1998)	N/A
pT25	(Karimova et al., 1998)	N/A
pT18-ubiA	This paper	N/A
pT18-ubiB	This paper	N/A
pT18-ubiC	This paper	N/A
pT18-ubiD	This paper	N/A
pT18-ubiE	This paper	N/A
pT18-ubiF	This paper	N/A
pT18-ubiG	This paper	N/A
pT18-ubiH	This paper	N/A
pT18-ubiI	This paper	N/A
pT18-ubiJ	This paper	N/A
pT18-ubiK	This paper	N/A
pT18-ubiX	This paper	N/A
pT25-ubiA	This paper	N/A
pT25-ubiB	This paper	N/A
pT25-ubiC	This paper	N/A
pT25-ubiD	This paper	N/A
pT25-ubiE	This paper	N/A
pT25-ubiF	This paper	N/A
pT25-ubiG	This paper	N/A
pT25-ubiH	This paper	N/A
pT25-ubiI	This paper	N/A
pT25-ubiJ	This paper	N/A
pT25-ubiK	This paper	N/A

pT25-ubiX	This paper	N/A
Software and Algorithms		
XDS	(Kabsch, 2010)	http://xds.mpimf-heidelberg.mpg.de/
STARANISO	(Bricogne et al., 2017)	http://staraniso.globalphasing.org/cgi-bin/staraniso.cgi
SHELXL	(Sheldrick, 2015)	http://shelx.uni-goettingen.de/
Coot	(Emsley et al, 2010)	https://www2.mrc-lmb.cam.ac.uk/personal/pemsley/coot/
BUSTER	(Bricogne et al., 2017)	https://www.globalphasing.com/buster/
CCP4	(Winn et al., 2011)	http://www.ccp4.ac.uk/
Pymol	Schrödinger, LLC	https://pymol.org/2/
CAVER3	(Chovancova et al., 2012)	https://www.caver.cz/
Mascot Distiller	Matrix Science	http://www.matrixscience.com/
Mascot	Matrix Science	http://www.matrixscience.com/
Proline	Open source	http://www.profiproteomics.fr/proline
Xcalibur	Thermo Fisher Scientific	https://www.thermofisher.com
Cytoscape 3.0	(Su et al., 2014)	https://cytoscape.org
Other		
Liquid chromatography	Thermo Scientific	UltiMate 3000 RSLCnano System
Reprosil-Pur 120 C18-AQ, 1.9 µm, 250 mm x 75 µm	Dr. Maisch GmbH	r119.aq.
Mass spectrometer	Thermo Scientific	Q Exactive Plus
BetaBasic-18, 150 mm x 4.6 mm, 5µm	Thermo Scientific	Cat# 71505-154630
Hitrap Chelating HP column	GE Healthcare	Cat# GE17-0408-01

FIGURE S1

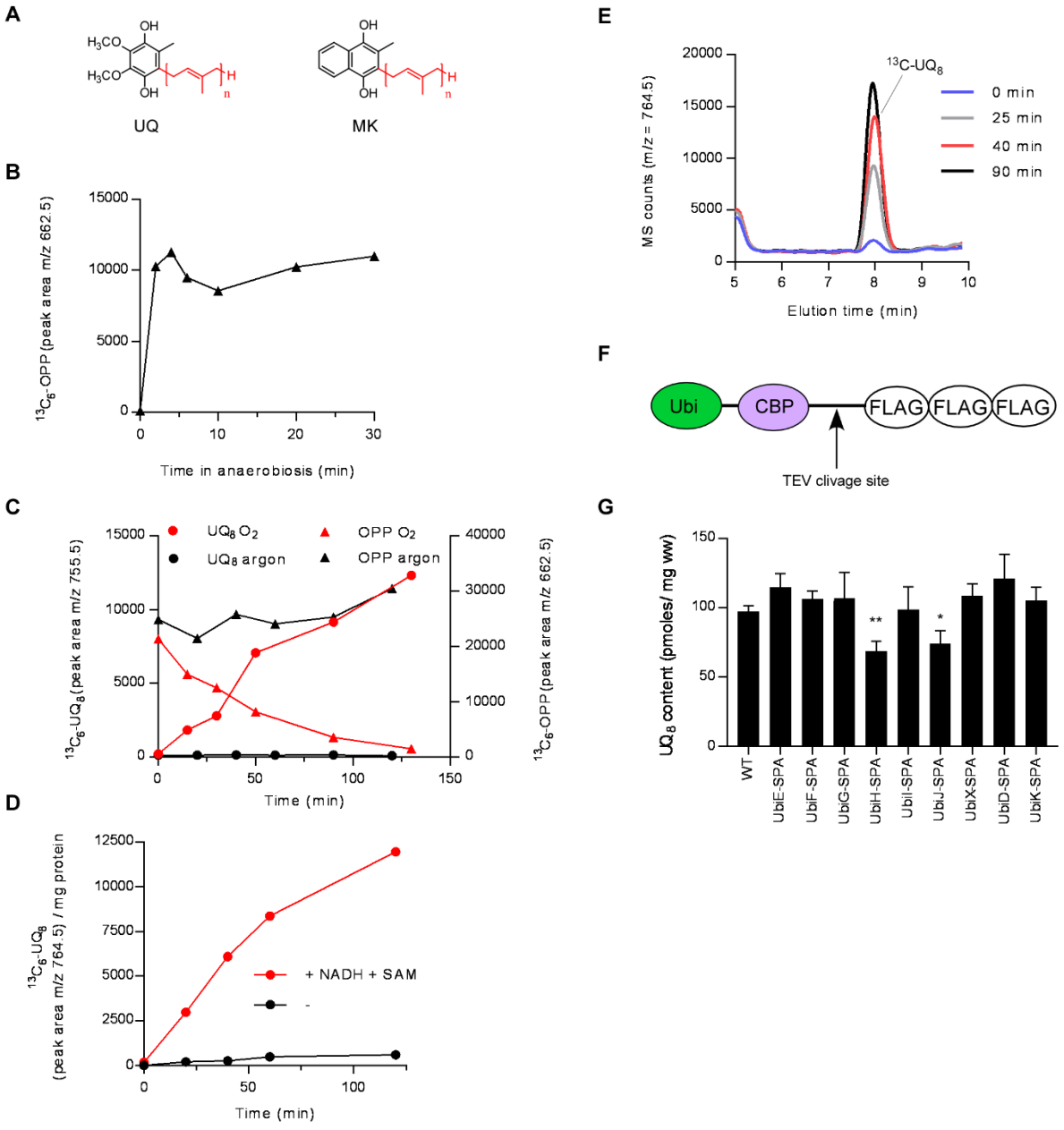

Figure S1 related to figure 1: A) Structures of Ubiquinone (UQ) and menaquinone (MK) with the head groups in black. The length of the polyprenyl tail (in red) can vary between species (n=6-10). B) Accumulation of $^{13}C_6$-OPP (M+ NH_4^+) after addition of $^{13}C_7$-4-HB to Δ*ubiC* cells incubated in anaerobic conditions. C) Conversion of $^{13}C_6$-OPP (M+ NH_4^+) into $^{13}C_6$-UQ_8 (M+ Na^+) by cells incubated in air or maintained under argon. D) Synthesis of $^{13}C_6$-UQ_8 (M+$CH_3NH_3^+$) by cell free extracts incubated in air with or without addition of NADH and SAM. E) HPLC analysis and single ion monitoring (m/z=764.5, M+$CH_3NH_3^+$) of $^{13}C_6$-UQ_8 in cytoplasmic fractions from Δ*ubiC* cells preloaded with ^{13}C-OPP and incubated in air for the

indicated time in the presence of NADH and SAM. Results shown are representative of two (B, C) or three independent experiments (D, E). F) Schematic representation of a Ubi protein fused to the SPA tag, a repetition of 3 FLAG sequences separated from a CBP (Calmodulin Binding Protein) domain by a TEV clivage site (TEV: Tobacco Etch Virus). G) HPLC-ECD quantification of cellular UQ_8 content of *E. coli* strains carrying Ubi proteins endogenously tagged with SPA (mean ±SEM, n=3, *: $p< 0.05$, **: $p< 0.01$, unpaired Student's t test). The UQ_8 decrease in UbiH-SPA and UbiJ-SPA cells is statistically significant but nevertheless reflects that the UbiH-SPA and UbiJ-SPA proteins remain partially functional since a complete inactivation would cause a lack of UQ_8, as observed in *ubiH* and *ubiJ* knock-out cells.

Figure S2

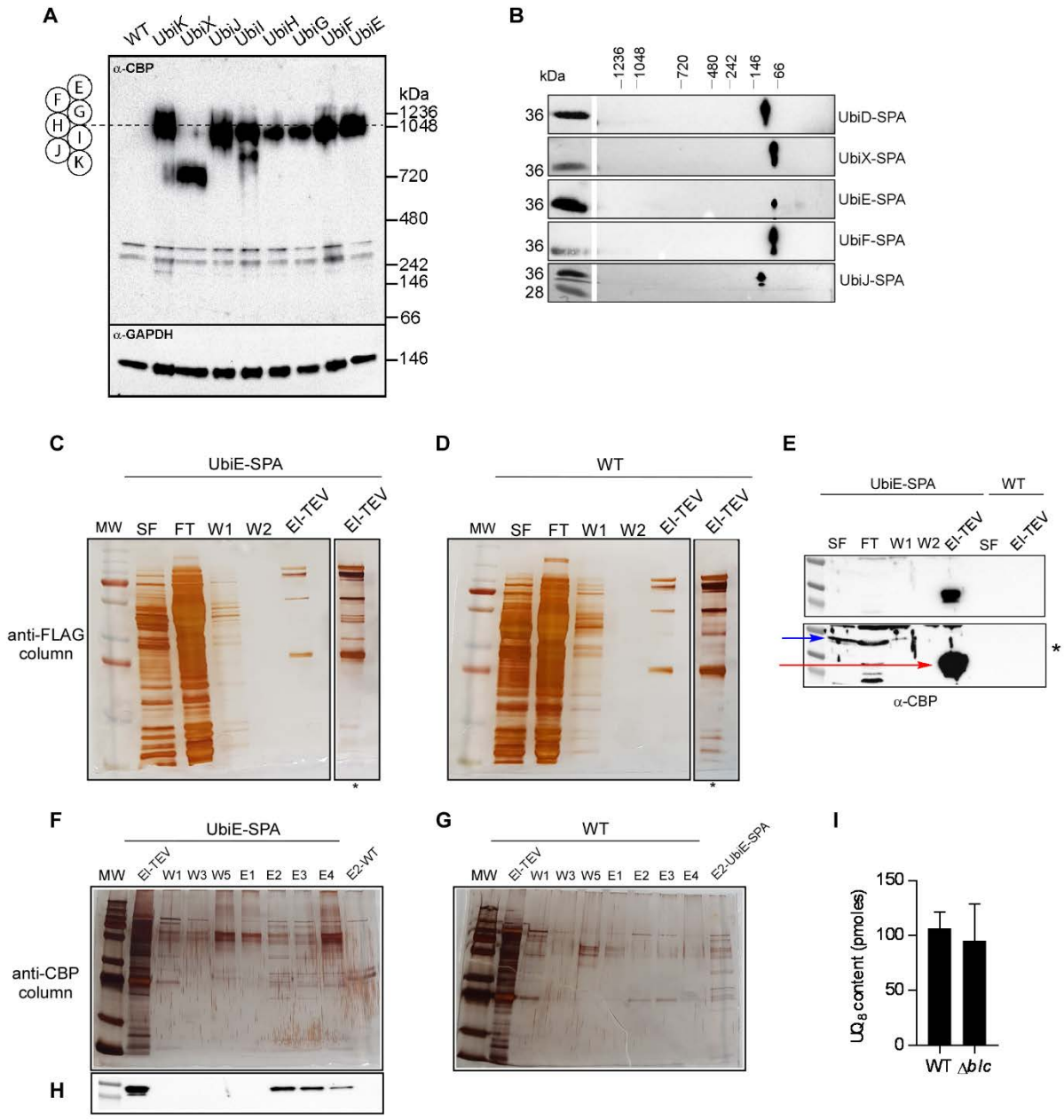

Figure S2 related to figure 2 and 3: A) BN-PAGE analysis and immunodetection of soluble fractions from the indicated Ubi-SPA strains (50 µg of total proteins). The membrane was first probed with α-CBP antibody, stripped and probed with α-GAPDH (loading control). B) Immunodetection of the control GAPDH protein after stripping the α-FLAG antibody from the membranes presented in Figure 2B. C-D) 20 uL aliquots of soluble fraction (SF), flow-through (FT), washes 1 and 2 (W1, W2), and eluates after TEV digestion (El-TEV) collected during the anti-FLAG purification step were analyzed by SDS-PAGE and the gel was colored by silver staining (extracts from the UbiE-SPA strain (C) and from the WT strain (D)). E)

Western-blot analysis with α-CBP antibody of samples described in C-D. Sizes of the UbiE-SPA protein before and after cleavage by TEV are indicated with blue and red arrows, respectively. Asterisks mark longer exposures (C-E). F-G) SDS-PAGE analysis and silver staining of fractions collected during the calmodulin purification step: washes 1, 3, 5 (W1, W3, W5) and eluates 1-4 (E1-E4) from purification with UbiE-SPA (F) and WT (G) samples. H) Western-blot analysis with α-CBP antibody of samples described in F. I) UQ_8 quantification in Δ*blc* and WT strains (mean ±SEM, n=4).

Figure S3

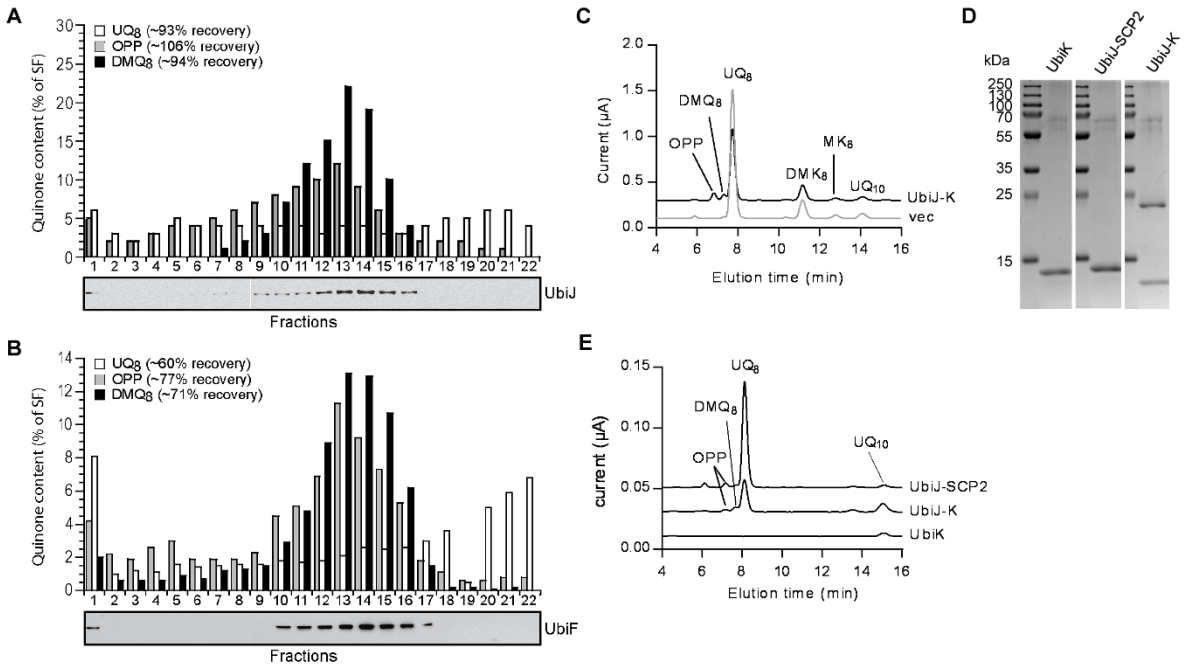

Figure S3 related to figure 4: A-B) Glycerol gradient analysis of soluble extracts from UbiJ-SPA and UbiF-SPA cells, and quantification of isoprenoid quinones in each fraction (see also Figure 4B). Western-blot are the same than in figure 2C. C) HPLC-ECD analyses (mobile phase 2) of lipid extracts from 1 mg of the *E. coli* cells containing an empty vector (vec) or overexpressing UbiJ(6His)-K and grown in LB medium (UQ_{10} used as standard), DMK_8 for C2-demethylmenaquinone 8. D) SDS-PAGE analysis and coomassie blue staining of purified UbiK, UbiJ-K and UbiJ-SCP2. E) HPLC-ECD analyses (mobile phase 2) of lipids extracted from 4 nmoles of purified proteins (UQ_{10} used as standard).

Figure S4

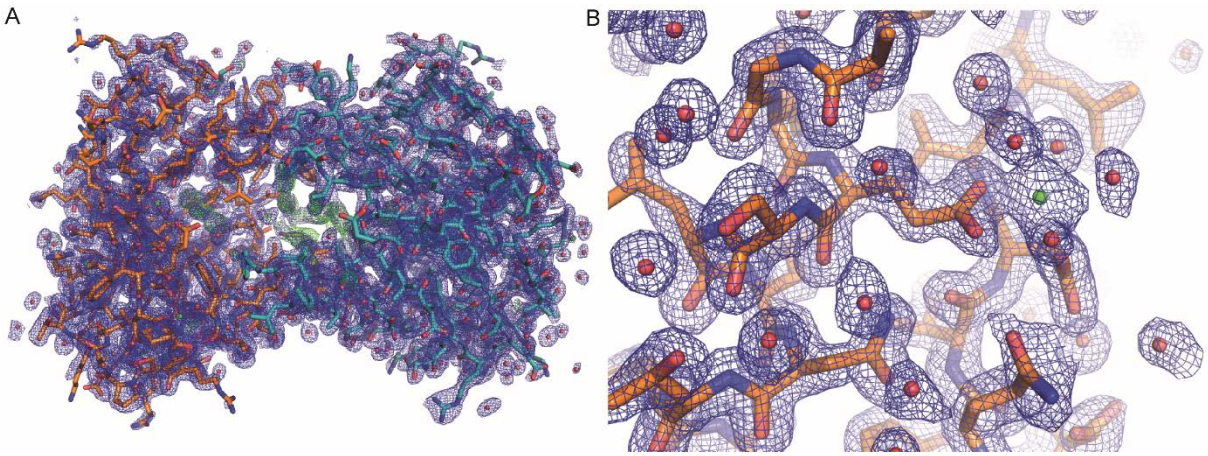

Figure S4 related to figure 5: Stick model of the structure of UbiJ-SCP2 at 1.7 Å resolution with electron density maps. A) UbiJ-SCP2 dimer with maps for 2FoFc set at 1 σ (blue mesh) and for FoFc set at 3 σ (green mesh). B) Zoomed in region of chain A with maps for 2FoFc set at 1 σ. (chain A shown in orange, chain B in teal, waters shown as red spheres, calcium shown as green spheres).

Figure S5

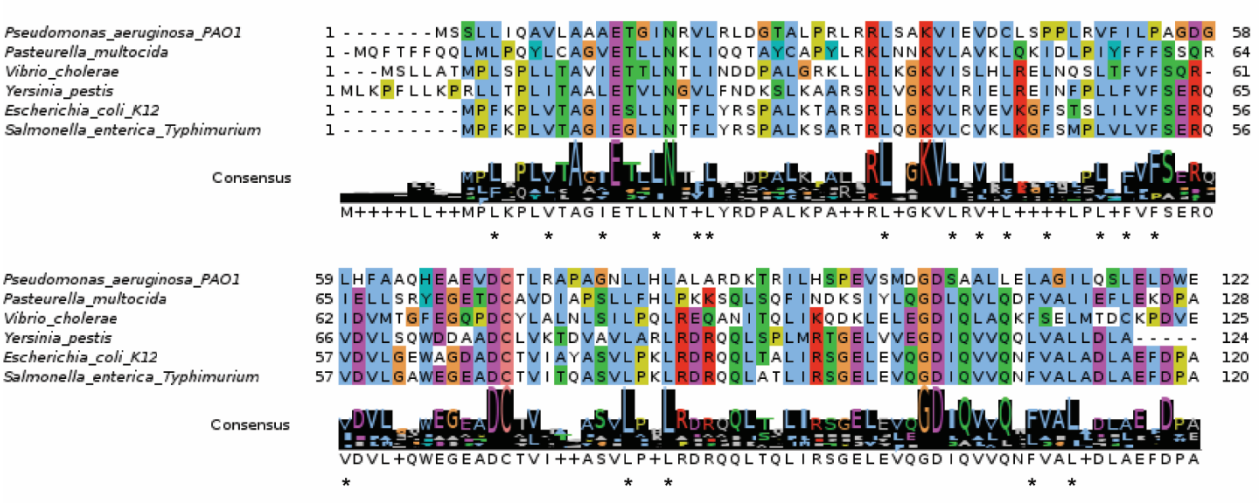

Figure S5 related to figure 5: Sequence alignment of UbiJ-SCP2 domains taken from various bacterial strains. Residues lining the hydrophobic cavity highlighted in figure 5c are indicated by *. NCBI sequence numbers: NP_253751.1, WP_005755273.1, NP_229743.1, NP_407227.1, NP_418278.1, NP_462856.1

Figure S6

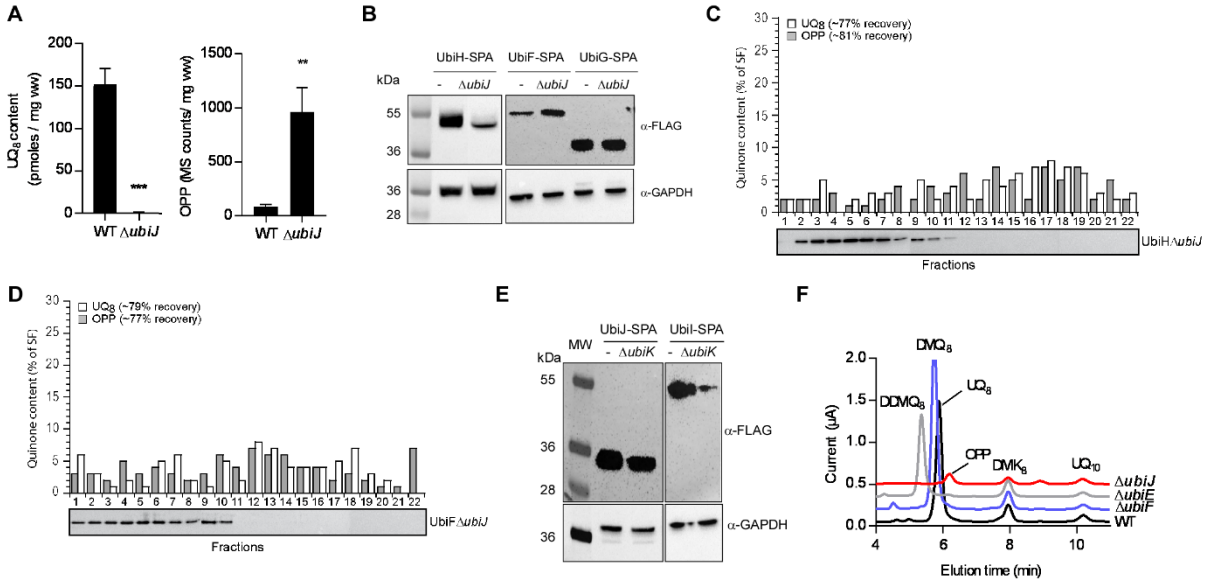

Figure S6 related to figure 6: A) UQ_8 and OPP content (normalized to cells wet weight) of WT and *ΔubiJ* cells grown in LB medium. B, E) Immunodetection of Ubi-SPA proteins (α-FLAG antibody) in the soluble fractions of the indicated strains (25 µg of proteins), with GAPDH as control. C-D) Glycerol gradient analysis of soluble extracts from UbiH-SPA *ΔubiJ* cells (C) or UbiF-SPA *ΔubiJ* cells (D) and quantification of OPP and UQ_8 in each fraction by HPLC-ECD-MS. Immunodetection with α-FLAG antibody showing the position UbiH-SPA and UbiF-SPA in fractions of the glycerol gradient (see also Figure 6A). F) HPLC-ECD analyses (mobile phase 1) of lipid extracts from 1 mg of the indicated *E. coli* cells grown in LB medium (UQ_{10} used as standard).

Table S1 related to figure 2E: Values of the bacterial two-hybrid assay, provided as separate excel file

Table S2 related to figure 3: Results of proteomic analysis, provided as separate excel file

Table S3 related to figure 5: Crystallography data table

Dataset	**Terbium**	**Native Dimer**	**Native Tetramer**
PDB code	6H6N	6H6O	6H6P
Space group	P 21 21 21	P 21 21 21	P 21 21 21
Unit cell dimensions			
a (Å)	48,3	48,66	47,69
b (Å)	67,93	67,87	94,55
c (Å)	73,08	74,61	115,66
Wavelength (Å)	1,6488	0,9786	0,9786
Resolution (Å)	40.29-2.11	39.55-1.70	47.28-2.5
Highest resolution bin (Å)	2.17-2.11	1.74-1.70	2.59-2.5
No. of reflections	307092	177660	137979
No. of unique reflections	13906	28017	18749
Completeness (%)	97.1 (60.7)	99.7 (96.7)	99.92 (99.94)
Rmerge	0.116 (0.709)	0.081 (1.957)	0.1602 (2.524)
I/σ (I)	12.3 (1.7)	10.7 (0.9)	9.13 (0.5)
CC1/2	0.998 (0.780)	0.999 (0.523)	0.998 (0.885)
Multiplicity	22.1 (9.3)	6.3 (6.1)	7.4 (7.7)
Refinement			
Rwork	0.194 (0.189)	0.202 (0.242)	0.233 (0.224)
Rfree	0.229 (0.227)	0.248 (0.271)	0.289 (0.258)
Average B-factor (Å2)			
Overall	43,05	32,65	79,12
From Wilson plot	32,35	22,83	72,21
No. of atoms			
Protein	1874	1851	3585
Water	118	185	89
RMS deviations from ideal			
Bond lengths (Å)	0,010	0,010	0,010
Bond angles (o)	1,07	0,98	1,27
Ramachandran outliers (%)			
Residues in most favored regions (%)	98,75	99,57	98,24
Residues in allowed regions (%)	1,25	0,43	1,76
Outliers (%)	0	0	0
*Values in parentheses are for the highest resolution bin.			

Table S4 related to figure 5: Structurally characterized SCP2 proteins and their structural alignment with UbiJ-SCP2

Protein	Organism	Technique	Resolution	PDB	RMSD	lipid content	Sequence coverage	Sequence Identity
Alkyl sulfatase	Pseudomonas sp. DSM 6611	X-ray Diffraction	2,7	2YHE	1,563	-	67	20
Alkyl sulfatase	Pseudomonas sp. DSM 6611	X-ray Diffraction	3	4AV7	2,138	-	67	20
SCP2	Human	X-ray Diffraction	1,75	1IKT	2,162	Triton X-100	83	14
SCP2	Archaeoglobus fulgidus	X-ray Diffraction	2,11	3BN8	2,241	-	81	11
Alkyl sulfatase	Pseudomonas sp. S9	X-ray Diffraction	1,761	4NUR	2,474	-	67	17
SCP2	Aedes aegypti	X-ray Diffraction	2	3BDQ	2,591	palmitic acid	90	18
SCP2	Helicoverpa armigera	NMR	n/a	4UEI	2,619	-	74	12
SCP2	Aedes aegypti	X-ray Diffraction	1,7	2QZT	2,983	palmitic acid	90	18
SCP2	Yeast Yarrowia Lipolytica	X-ray Diffraction	2,2	4JGX	3,402	palmitic acid	79	14
SCP2	Oryctolagus cuniculus	X-ray Diffraction	1,8	1C44	3,483	-	68	18
SCP2	Homo sapiens	NMR	n/a	1QND	3,854	-	68	17
-	Archaeoglobus fulgidus	X-ray Diffraction	1,9	3CNU	4,084	-	90	11
SCP2	Aedes aegypti	NMR	n/a	2NBM	4,473	-	85	18

Table S5 related to figure 1, 2: *E. coli* strains used in this study

strain	type	relevant genotype	source or reference
BW25113		*lacI^q rrnB$_{T14}$ lacZ$_{WJ16}$ hsdR514 araBAD rhaBAD$_{LD78}$*	National BioResource Project
MG1655		Wild type	ATCC
BTH101		*F', cya-99, araD139, galE15, galK16, rpsL1 (Str^R), hsdR2, mcrA1, mcrB1*	Karimova *et al*, 1998
DY330		W3110 ΔlacU169 gal490 λCI857 Δ(cro-bioA)	Hu *et al*, 2009
BL21 (DE3)		*fhuA2 [lon] ompT gal (λ DE3) [dcm] ΔhsdS λ DE3*	Merck Millipore
	Keio strains		*Keio* collection (Baba *et al*, 2006)
BW25113		*lacI^q rrnB$_{T14}$ lacZ$_{WJ16}$ hsdR514 araBAD rhaBAD$_{LD78}$*	Laboratory collection
BW25113 Δ*ubiC*		As BW25113 but Δ*ubiC*::Kan	JW5713
BW25113 Δ*ubiE*		As BW25113 but Δ*ubiE*::Kan	JW5581
BW25113 Δ*ubiF*		As BW25113 but Δ*ubiF*::Kan	JW0659
BW25113 Δ*ubiG*		As BW25113 but Δ*ubiG*::Kan	JW2226
BW25113 Δ*blc*		As BW25113 but Δ*blc*::Kan	JW4110
	Knock-out strains		
MG1655 Δ*ubiE*		As MG1655 but Δ*ubiE*::Kan	Hajj Chehade *et al*, 2013
MG1655 Δ*ubiF*		As MG1655 but Δ*ubiF*::Kan	Hajj Chehade *et al*, 2013
MG1655Δ*ubiJ*		As MG1655 but Δ*ubiJ*::Kan	Aussel *et al*, 2014
	SPA-strains		
DY330		W3110 ΔlacU169 gal490 λCI857 Δ(cro-bioA)	Hu *et al*, 2009
DY330 *ubiC*-SPA		As DY330 but *ubiC*-SPA::Kan	GI number 90111677
DY330 *ubiF*-SPA		As DY330 but *ubiF*-SPA::Kan	GI number 16128645
DY330 *ubiG*-SPA		As DY330 but *ubiG*-SPA::Kan	GI number 16130167
DY330 *ubiH*-SPA		As DY330 but *ubiH*-SPA::Kan	GI number 16130809
DY330 *ubiX*-SPA		As DY330 but *ubiX*-SPA::Kan	GI number 16130246
BW25113 *ubiD*-SPA		As BW25113 but *ubiD*-SPA::Kan	this work
BW25113 *ubiI*-SPA		As BW25113 but *ubiI*-SPA::Kan	this work
MG1655 *ubiC*-SPA		MG1655 +P1/DY330 *ubiC*-SPA::Kan	this work
MG1655 *ubiD*-SPA		MG1655 +P1/BW25113 *ubiD*-SPA::Kan	this work
MG1655 *ubiE*-SPA		*ubiE*-SPA::Kan	Loiseau *et al*, 2017
MG1655 *ubiF*-SPA		MG1655 +P1/DY330 *ubiF*-SPA::Kan	this work
MG1655 *ubiG*-SPA		MG1655 +P1/DY330 *ubiG*-SPA::Kan	this work
MG1655 *ubiH*-SPA		*MG1655 +P1/*DY330 *ubiH*-SPA::Kan	this work
MG1655 *ubiI*-SPA		MG1655 +P1/BW25113 *ubiI*-SPA::Kan	this work
MG1655 *ubiJ*-SPA		*ubiJ*-SPA::Kan	Loiseau *et al*, 2017
MG1655 *ubiK*-SPA		*ubiK*-SPA::Kan	Loiseau *et al*, 2017
MG1655 *ubiX*-SPA		*MG1655 +P1/DY330 ubiX*-SPA::Kan	this work
MG1655 *ubiH*-SPA Δ*ubiE*		Δ*ubiE* (cured with pCP20) + P1/ubiH-SPA::Kan	this work
MG1655 *ubiH*-SPA Δ*ubiF*		Δ*ubiF* (cured with pCP20) + P1/ubiH-SPA::Kan	this work
MG1655 *ubiH*-SPA Δ*ubiG*		Δ*ubiG* (cured with pCP20) + P1/ubiH-SPA::Kan	this work
MG1655 *ubiH*-SPA Δ*ubiJ*		Δ*ubiJ* (cured with pCP20) + P1/ubiH-SPA::Kan	this work
MG1655 *ubiF*-SPA Δ*ubiJ*		Δ*ubiJ* (cured with pCP20) + P1/ubiF-SPA::Kan	this work
MG1655 *ubiG*-SPA Δ*ubiJ*		Δ*ubiJ* (cured with pCP20) + P1/ubiG-SPA::Kan	this work
MG16555 *ubiI*-SPA Δ*ubiK*		Δ*ubiK* (cured with pCP20) + P1/ubiI-SPA::Kan	this work
MG1655 *ubiJ*-SPA Δ*ubiK*		Δ*ubiK* (cured with pCP20) + P1/ubiJ-SPA::Kan	this work
MG1655 *ubiE*-SPA Δ*ubiC*		Δ*ubiK* (cured with pCP20) + P1/ubiE-SPA::Kan	this work

Table S6 related to figure 1: Oligonucleotides used in this study

name	category	sequence
	SPA-tag	
5-ubiD-SPA		attgacgccatctgggatgaactggctatttttaacaacggtaaaagcgccTCCATGGAAAAGAGAAG
3-ubiD-SPA		catgcgctttctctgtcggatcgataaatagggcaaaacaaacgcgcatcaCATATGAATATCCTCCTTAG
5-ubiE-SPA		cgactactacaatctgacggcaggggttgtggcgctgcatcgtggttataagttcTCCATGGAAAAGAGAAG
3-ubiE-SPA		cctgccgtcactaaaggtttaaaaggcatttccggtctcctgtcaCATATGAATATCCTCCTTAG
5-ubiI-SPA		atccgccaggcaatgggattaaacgatttgcctgaatggctgcgtTCCATGGAAAAGAGAAG
3-ubiI-SPA		gatgaaagtgtgatgggtatcaaataaacaacagaggagaaatttttaCATATGAATATCCTCCTTAG
5-ubiJ-SPA		gctgttgatgccctgaccaaacggctggaaaaactggaggctaaaTCCATGGAAAAGAGAAG
5-ubiJ-SPA		agtgcgaatgatgaaatataggcgccgtacttcacctggcgtcatttagcctccttaCATATGAATATCCTCCTTAG
5-ubiK-SPA		gagatcaaaaagcagccagatccagagactctccccccaacgctgTCCATGGAAAAGAGAAG
3-ubiK-SPA		ttagaggattaattcataatttacagtgcattaaagacgaatgtttaCATATGAATATCCTCCTTAG
5-atpB SPA		ttcatggttctgacgatcgtctatctgtcgatggcgtctgaagaacatTCCATGGAAAAGAGAAG
3-atpB SPA		ttttccatgacagtctccagtttgtttcagttaaaacgtagtagtgttggtaaaCATATGAATATCCTCCTTAG
	bacterial two-hybrid	
5xbaI-ubiA		GACTCTAGAGATGgagtggagtctgacgc
3xbaI-ubiA		TCCGTCTAGAtcagaaatgccagtaactcattgcc
5xbaI-ubiB		TCGACTCTAGAGATGACGCCAGGTGAAGTACGGCGC
3xbaI-ubiB		CTTCCGTCTAGATCAGCGTGTTTTGCGCCAACCGACAAACCAGG
5xbaI-ubiC		TCGACTCTAGAGATGtcacaccccgcgttaacgcaactg
3xbaI-ubiC		CTTCCGTCTAGATTAgtacaacggtgacgcc
5xbaI-ubiD		TCGACTCTAGAGatggacgccatgaaatataacgatttacgc
3xbaI-ubiD		CTTCCGTCTAGAtcaggcgcttttaccgttgttaaaaatagccagttcatcc
5xbaI-ubiE		TCGACTCTAGAGATGGTGGATAAGTCACAAGAAACGAC
3xbaI-ubiE		CTTCCGTCTAGATCAGAACTTATAACCACGATGCAGCGC
5xbaI-ubiF		TCGACTCTAGAGATGACAAATCAACCAACGGAAATTGC
3xbaI-ubiF		CTTCCGTCTAGACTACAACCCTAACGCATATTTCAGC
5xbaI-ubiG		TCGACTCTAGAGATGaatgccgaaaaatcgccggtaaaccataacgtagac
3xbaI-ubiG		CTTCCGTCTAGAtcacttattctgcgtgtgcagcatatagttcac
5xbaI-ubiH		GACTCTAGAGATGagcgtaatcatcgtcgg
3xbaI-ubiH		TCCGTCTAGAtcaacgcgccacccaaccgagggtgcgc
5xbaI-ubiI		TCGACTCTAGAGATGCAAAGTGTTGATGTAGCC
3xbaI-ubiI		CTTCCGTCTAGATTAACGCAGCCATTCAGGCAAATC
5xbaI-ubiJ		TCGACTCTAGAGATGCCTTTTAAACCTTTAGTGACG
3xbaI-ubiJ		CTTCCGTCTAGATCATTTAGCCTCCAGTTTTTCCAGCCG
5xbaI-ubiK		TCGACTCTAGAGATGATTGACCCGAAAAAAATTGAG
3xbaI-ubiK		CTTCCGTCTAGATTACAGCGTTGGGGGGAGAG
5xbaI-ubiX		TCGACTCTAGAGATGAAACGACTCATTGTAGGCATCAG
3xbaI-ubiX		CTTCCGTCTAGATTATGCGCCCTGCCAGCG

Click here to access/download

Supplemental Videos and Spreadsheets

Table S1.xlsx

Click here to access/download

Supplemental Videos and Spreadsheets

Table S2.xlsx